THE ANATOMICAL RECORD 291:353–378 (2008)

Anatomic Geometry of Sound Transmission and Reception in Cuvier's Beaked Whale (*Ziphius cavirostris*)

TED W. CRANFORD,[1]* MEGAN F. MCKENNA,[2] MELISSA S. SOLDEVILLA,[2] SEAN M. WIGGINS,[2] JEREMY A. GOLDBOGEN,[2] ROBERT E. SHADWICK,[2] PETR KRYSL,[3] JUDY A. ST. LEGER,[4] AND JOHN A. HILDEBRAND[2]

[1]San Diego State University and Quantitative Morphology Consulting, Inc., San Diego, California
[2]Scripps Institution of Oceanography, San Diego, California
[3]University of California at San Diego, San Diego, California
[4]SeaWorld San Diego, San Diego, California

ABSTRACT

This study uses remote imaging technology to quantify, compare, and contrast the cephalic anatomy between a neonate female and a young adult male Cuvier's beaked whale. Primary results reveal details of anatomic geometry with implications for acoustic function and diving. Specifically, we describe the juxtaposition of the large pterygoid sinuses, a fibrous venous plexus, and a lipid-rich pathway that connects the acoustic environment to the bony ear complex. We surmise that the large pterygoid air sinuses are essential adaptations for maintaining acoustic isolation and auditory acuity of the ears at depth. In the adult male, an acoustic waveguide lined with pachyosteosclerotic bones is apparently part of a novel transmission pathway for outgoing biosonar signals. Substitution of dense tissue boundaries where we normally find air sacs in delphinoids appears to be a recurring theme in deep-diving beaked whales and sperm whales. The anatomic configuration of the adult male *Ziphius* forehead resembles an upside-down sperm whale nose and may be its functional equivalent, but the homologous relationships between forehead structures are equivocal. Anat Rec, 291:353–378, 2008.

Key words: anatomic geometry; quantitative morphology; X-ray CT; beaked whale; biosonar; *Ziphius*; cephalic; Cuvier

Beaked whales (Family: Ziphiidae) are a group of large- to medium-sized toothed whales composed of twenty one species world wide. Anecdotes from 17th century hand-whalers told of prodigious diving in beaked whales, a capacity that is only now being confirmed with the development and use of tags containing time-depth recorders (Hooker and Baird, 1999; Johnson and Tyack, 2003a; Johnson et al., 2006; Tyack et al., 2006).

Almost nothing is known about the *form* of large whales. It is this *form* that is the primary interface between an organism and its environment. It is this *form* that combines with tissue properties to determine acoustic pathways and conditions throughout the head. But, the terms *form*, *anatomy*, and *morphology* are traditional synonyms that generally refer simply to the biological structure, knowledge that has historically been gathered using dissection by hand. In the current treatment, these terms seem somewhat insufficient or incomplete, because they do not emphasize or reveal that the "geometry" of anatomic structure is accessible in the digital remote images presented here. This in situ

*Correspondence to: Ted W. Cranford, Department of Biology, San Diego State University, San Diego, CA.
E-mail: tcranfor@mail.sdsu.edu

Received 27 June 2007; Accepted 12 November 2007
DOI 10.1002/ar.20652
Published online 29 January 2008 in Wiley InterScience (www.interscience.wiley.com).

"anatomic geometry" has not been available before the use of remote imaging technology and is perhaps the most important component in constructing and understanding biosonar acoustic pathways (Aroyan et al., 1992; Cranford et al., in press).

The purpose of this study is to provide the first high-fidelity anatomic images and geometric descriptions of the structures associated with the biosonar apparatus in Cuvier's beaked whale (*Ziphius cavirostris*), the only species within this genus. The catalyst for this work is the high number of cetaceans, beaked whales in particular, that have stranded in association with exposure to high-intensity sounds (Evans and England, 2001). Cuvier's beaked whale accounts for the majority of specimens stranded in the events reported thus far.

The cephalic anatomy of the odontocete head and its acoustic function has been the subject of naturalists' curiosity and research over the past century. Reviews of this work can be found in Mead (1975), Heyning (1989b), Cranford (1992, 2000), and Cranford and Amundin (2003). The most recent review (Cranford and Amundin, 2003) describes what we know about the pneumatic mechanism of sonar signal generation and sound transmission in toothed whales. It also concludes that the "unified hypothesis" of Cranford et al. (1996) is valid. Their unified hypothesis states that all odontocetes generate their sonar signals by a similar mechanism at homologous location(s). The site of sound generation has been identified as the "phonic lips" (Cranford, 1999), formerly known as the "museau de singe" (Pouchet and Beauregard, 1885) or "monkey-lip dorsal bursae" complex or simply the MLDB complex (Cranford et al., 1996). The "anatomic complex" includes the lips and a set of accessory structures that are apparently common to all odontocetes.

Our detailed study of *Ziphius cavirostris* cephalic anatomy will focus upon the nasal anatomy, containing the sound generation apparatus, and the peripheral hearing apparatus. This suite of structures comprises the biosonar apparatus in *Z. cavirostris*. Increased knowledge of the structure and the function of this apparatus may advance our understanding of the causal effects surrounding mass stranding of *Z. cavirostris* in the presence of mid-frequency sonar (Cox et al., 2006).

Recent advancements in industrial computed tomography (CT), allowed scanning of large fusiform biological specimens. Industrial CT captures and stores high-fidelity digital representations of morphology based upon X-ray absorption, a quantity related to electron density or simply density (Bushberg et al., 2001). A detailed description of the scanning process for large whales using industrial CT will be described elsewhere.

After scanning, the anatomic geometry becomes accessible through a wide array of image processing tools and techniques. These techniques provide unprecedented flexibility in transformation of scale between the investigator and the specimen. As such, a leviathan can be seen in its entirety, from any angle or perspective, or manipulated with respect to structures displayed, color, or transparency. These tools provide access to the most important results from this work, the descriptive and quantitative characterizations of the basic components of the biosonar apparatus and its accessory structures in *Z. cavirostris*. This is the first quantitative description of anatomic geometry for this species. Because *Ziphius* is a monotypic genus, from here forward, we will refer to Cuvier's beaked whale simply as *Ziphius*.

The interpretive power in this work accrues from two types of comparisons. First, we consider the similarities and differences between anatomy of the biosonar apparatus in two specimens of *Ziphius*, a neonate female and an adult male. Second, we draw upon comparisons across the entire suborder, from odontocete specimens in existing digital libraries and museum collections, particularly those at the Smithsonian Institution in Washington, DC.

Because most of the results reported here are quantitative, we will also attempt to specify the error and bias in observers trained to make the measurements (shown in Table 2). In this case, we used comparisons from measurements of the tympanoperiotic complex within the hearing apparatus of *Ziphius*.

Beyond the implications for functional morphology, there are also intriguing phylogenetic considerations that follow from our results and they will find their way into the Discussion section. In particular, it is generally accepted that the evolutionary restructuring of the face of the odontocete skull and the hypertrophy of the nasal soft tissues is largely due to the development of the signal generation and transmission portion of the biosonar apparatus (Norris, 1964, 1968, 1969, 1975; Cranford, 1992, 2000; Cranford and Amundin, 2003). In addition, there is apparently an "acoustic" component to the sexually dimorphic forehead anatomy and corresponding sexual selection (Cranford, 1999) in odontocetes. This issue will also be explored briefly in the discussion of *Ziphius* forehead anatomy. Furthermore, a discussion of the structure of the sound reception apparatus on the ventral aspect of the head will address adaptations associated with deep diving.

MATERIALS AND METHODS

Specimens

***Neonate female* Ziphius cavirostris (*Zica Neo F*).** A neonate female *Ziphius cavirostris* stranded alive at Camp Pendleton, California, on 7 January 2002 (NMFS Field # KXD0019). The animal was 3.15 m long, weighed 363 kg (800 pounds), and was placed in a freezer within 15 hours of its death. The pathology report indicated that this newborn probably died after being separated from its mother and did not show any outward signs of disease, hemorrhage, or injury. The frozen specimen was enclosed in a large plastic pipe, the primary component of a registration frame-of-reference that also contains known density rods attached in parallel along the length of the pipe. A polyurethane (two-part) foam matrix was poured to fill in the empty volume and bind the specimen to the wall of the pipe. The entire container (including the specimen) was cut into four, more or less, equivalent mass segments. Each segment was scanned with X-ray CT using a 512 matrix size and 5 mm "slice" thickness. The section containing the head was also scanned using magnetic resonance imaging (MRI) but these results will be reported elsewhere. Standard hospital CT equipment (e.g., GE Lightspeed scanner) was used to scan this neonate.

After scanning, each of the four major sections from this neonate beaked whale was subjected to dissection

followed by sound propagation measurements of extracted tissue samples (Soldevilla et al., 2005). (Details of scanning protocols, dissection, and sampling procedures can be found in Soldevilla et al. [2005] and Boisvert [2004]). This report includes anatomic information regarding the head of this neonate specimen, to the exclusion of the postcranial anatomy.

Adult male* Ziphius cavirostris *(Zica Adult M). An adult male *Ziphius cavirostris* stranded alive at Gearhart Beach, Oregon, on 13 March 2002. The animal died soon thereafter and was collected by Portland State University (Field # PSU 3-13-02 Zc, NMFS Reg. No. 02NWR03004). It measured 5.15 m long and weighed 1,996 kg (4,400 pounds). After stranding in the late afternoon, the animal's head was covered with ice overnight, disarticulated from the body the following morning, and put into a freezer. This series of actions guaranteed that the head of this adult male *Z. cavirostris* was in excellent condition and provided an opportunity to get the first quantitative look into the in situ anatomic geometry.

The size, weight, coloration, and characteristic scarring by the teeth of conspecifics caused experienced observers to classify this male *Z. cavirostris* as an adult. Heyning's (1989a) overview of what was known about *Z. cavirostris* includes a review of the literature. He found that Omura et al. (1955) reported the mean length for sexually mature males is 5.50 m for at least some stocks of western north Pacific *Z. cavirostris*. This puts our specimen within the range of adult specimens. There were no outward signs that this specimen might have stranded as a result of exposure to high-intensity sound (Evans and England, 2001; Rommel et al., 2006). However, we did find some blood in the bony nasal passages but could not identify its source. The length of this specimen was the same as the modal size for *Ziphius* specimens that have died in mass strandings associated with exposure to Navy sonar operations (MacLeod and D'Amico, 2005).

To collect scan data for the adult male *Ziphius*, we used a large industrial CT scanner in a manner similar to that reported by Cranford (1999). The details of the unique construction of the sarcophagus for scanning will be reported elsewhere (Cranford, manuscript under review). The frozen specimen is placed in a fiberboard tube and encased in two component polyurethane foam (made by combining an isocyanate [A] component with a polyol [B] component). Exactly 373 transverse scans or "slices" of 2.5-mm thickness were collected using a square matrix of 1,024 and a field of view (FOV) of 1,350 mm, which translates to voxel dimensions of 1.3 mm $\times$ 1.3 mm $\times$ 2.5 mm. All scan data slices were loaded into the Analyze image processing software package and interpolated using a cubic spline algorithm to produce a volume composed of cubic voxels that were 1.5 mm on each side. This volume was used to glean the results reported here. The Analyze environment allowed us to separate or "segment" the entire volume of the head into various structures. It also provided a means to display, measure, and calculate linear and angular dimensions, as well as, volumes, densities, gradients, surfaces, shape parameters, and spatial relationships.

We collected a second set of scans with finer resolution over the region of the head containing the ears of this adult male specimen. For the ears, we used a square matrix of 2,048 and the same FOV (1,350 mm) along with a 1.3 mm slice thickness. This resulted in voxels with dimensions of 0.6 mm $\times$ 0.6 mm $\times$ 1.3 mm. A cubic spline interpolation of all these scans produced cubic voxels with 0.6 mm on each side, and this volume was used in our analysis.

We eventually took this specimen to the exquisite dissection facilities at the Smithsonian Institution. Beyond ground-truthing the CT scan information, we decided to pay particular attention to the morphology of two adjoining spaces, the pterygoid sinus and the fibrous venous plexus (FVP). In a dead specimen, the pterygoid sinus is large and cavernous, whereas the FVP is usually devoid of fluid and somewhat flattened along its length anteriorly (Fig. 12). During the dissection, we devised a means to facilitate following the pathways and complex architecture of the pterygoid sinuses (as well as the posterior peribullary sinuses connected to it) and the fibrous venous plexus. After exposing the anteroventral boundaries of these complex cavities, we propped the head on the occipital condyles so that the rostrum pointed up (perpendicular to the table) and opened a small hole in each cavity. Then we injected warm solutions of different colored gelatin (Jello) into each and allowed them to solidify. This allowed us to follow the complex structure of these adjacent cavities throughout the dissection without confusing them.

Density Conversion

To ensure that each scan included fiduciary points and standard density references, we placed a set of parallel rods within the scanned package. These rods function as a "density phantom" and registration frame. We used four different 2-inch-diameter rods: Polycarbonate, Acetal Copolymer, high-density polyethylene (HDPE), and Fluoropolymer–Virgin Electrical Grade Teflon® (PTFE). These compounds span the density range of most biological tissue. We clipped a sample from the end of each rod, measured its volume by displacement, and weighed it on an analytical balance to ascertain the precise density of our rods. This allowed us to construct a linear regression between CT number (CT#) and density (as shown in Fig. 1a,b; Density Conversion Charts).

Measurements of Error and Bias

Our digital data sets were collected as a series of two-dimensional (2D) images perpendicular to the long axis of the body. These images have a "thickness" (the width of the X-ray beam) and can be appended to one another to reconstruct a 3D volume (Fig. 2). Once reconstructed the anatomic geometry can be segmented, measured, manipulated, or output (in parts or in whole) for scientific visualization, morphometric analysis, rapid prototyping, finite element modeling, and a wide array of other applications. The essential process that all others follow from is known as "segmentation."

Segmentation requires a human operator to make decisions about where to draw boundaries between structures, that is, which voxels will be included or excluded from the definition of any particular structure. This process is more difficult than it might first appear because tissue boundaries are most often gradients that are rarely precipitous. In addition, when interpreting

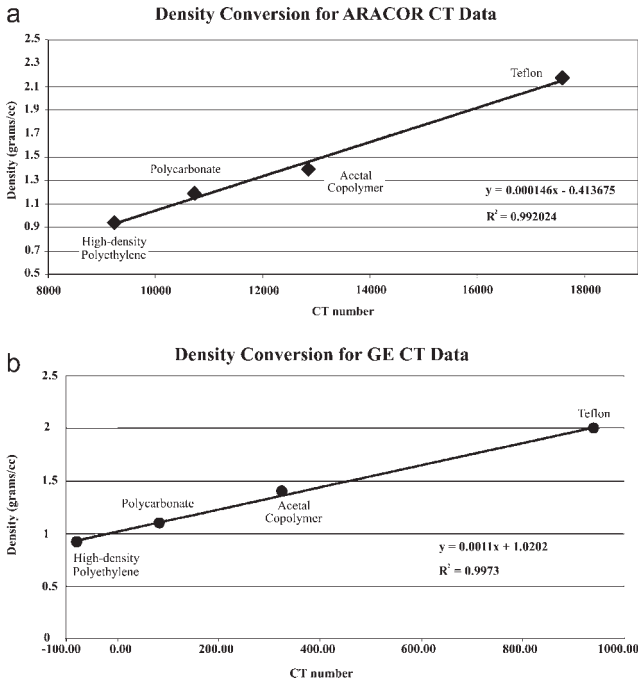

Fig. 1. **a:** Density conversion chart for the adult male *Ziphius*. The equation for conversion and correlation coefficient are given. **b:** Density conversion chart for the neonate female *Ziphius*. The equation for conversion and correlation coefficient are given.

any remote imaging scans from rare species or unique specimens, dissection is always required to help ground-truth the scans. Segmentation is often accomplished with the assistance of computer tools like digital thresholding that help make consistent decisions about defining boundaries. There are at least two sources of error or variation inherent in our ability to define boundaries and make measurements. The first is referred to as "observer bias." This type of error grows out of the relative skill levels, anatomic knowledge, judgments, and decisions made when human operators are involved in the segmentation process. It is difficult to put exact numbers on observer bias, because it is dependent upon which structure is being segmented and on anatomic knowledge of the species. For example, it is much easier to choose a boundary between bone and soft tissue than one between two soft tissue structures. This finding is primarily a function of the steepness of the density gradient between the two structures that are being segmented from one another (McKenna, 2005; McKenna et al., 2007). This means that segmentation of the high-density tympanoperiotic complexes should be the easiest to attain consistently and should yield the smallest human errors using any method.

The other source of error is based upon the machines and algorithms used to gather, process, and display the information (Robb, 1995, 2000). These errors have been greatly minimized in modern medical imaging equipment and quantifying them depends upon the specific equipment and software, but it is important to be aware of potential errors so that they can be recognized when they occur. It is also important to note that these "machine" errors can be amplified or exaggerated when the structures to be segmented are large relative to the matrix size and/or corresponding voxel dimensions, when the steepness of the gradient between adjacent tissues is high, the "slice" thickness or X-ray beam width over which complex averaging takes place is small, or when the algorithms used to process the raw data are not optimal for the desired information, that is, when a soft tissue algorithm is used to collect information about bony boundaries (Spoor et al., 1993; Bushberg et al., 2001). An attempt to quantify observer bias and the magnitude of machine error in our measurements is tabulated in Table 2.

RESULTS

The Biosonar Apparatus

The biosonar apparatus includes sound generation and transmission structures on the dorsal surface of the concave face of the skull (Cranford et al., 1996). It also includes the peripheral sound reception components associated with the mandibles and the presumed hearing apparatus located in two large furrows that run between the skull and the mandibles on each side of the ventral aspect of the head (Norris, 1969; Ketten, 2000). The following sections will provide the anatomic results for these two major subdivisions of the sonar apparatus.

Sound transmission anatomy of the forehead. The specific epithet, *cavirostris*, for Cuvier's beaked whale refers to the "hollow" or "concavity," termed the *prenarial basin* in the skull of adult males. This cavity appears as a depression in the bones on the superior aspect of the skull just anterior to the superior bony nares (Figs. 3, 5, 10). This region, the odontocete forehead, is the site of sonar signal generation (Norris and Evans, 1967; Norris, 1969, 1975; Ridgway et al., 1980; Amundin and Andersen, 1983; Amundin, 1991; Cranford et al., 1996), sound propagation pathways (Au et al., 1978; Au et al., 1988), and sonar beam formation (Au et al., 1986, 1995, 2006; McKenna, 2005).

The CT scans of our adult male *Ziphius* show that the prenarial basin of the skull is formed by three bony elements (premaxillary, maxillary, and vomer; Fig. 4). The vomer forms a portion of the floor of the basin along most of its length. The premaxillary bones appear to be pushed aside, away from the midline and thrust somewhat dorsally to form a high-density bony wall that embraces a large fat body laterally and incompletely along the ventral margin (Fig. 3). The remaining ventral margin of the fat body is just dorsal to the vomer. In cross-section, the resultant bony formation is reminiscent of the U-shaped valleys formed by the scouring action of mountain glaciers. The steep vertical walls (formed by the premaxillary and maxillary bones) are thicker and more uniform on the left than on the right (Fig. 3). The nasal bones are similarly high-density elements that are continuous with the bones that comprise the prenarial basin, but curiously, they hang over the prenarial basin rather than form part of it (Fig. 4).

There is another interesting feature of the embracing bones of the forehead region in the adult male *Ziphius*. The bony constituents (premaxillary, maxillary, vomer, and nasal bones) of the face are apparently *pachyosteosclerotic*. That is, the bones tend to be thicker than usual, and trabecular bone has been replaced by com-

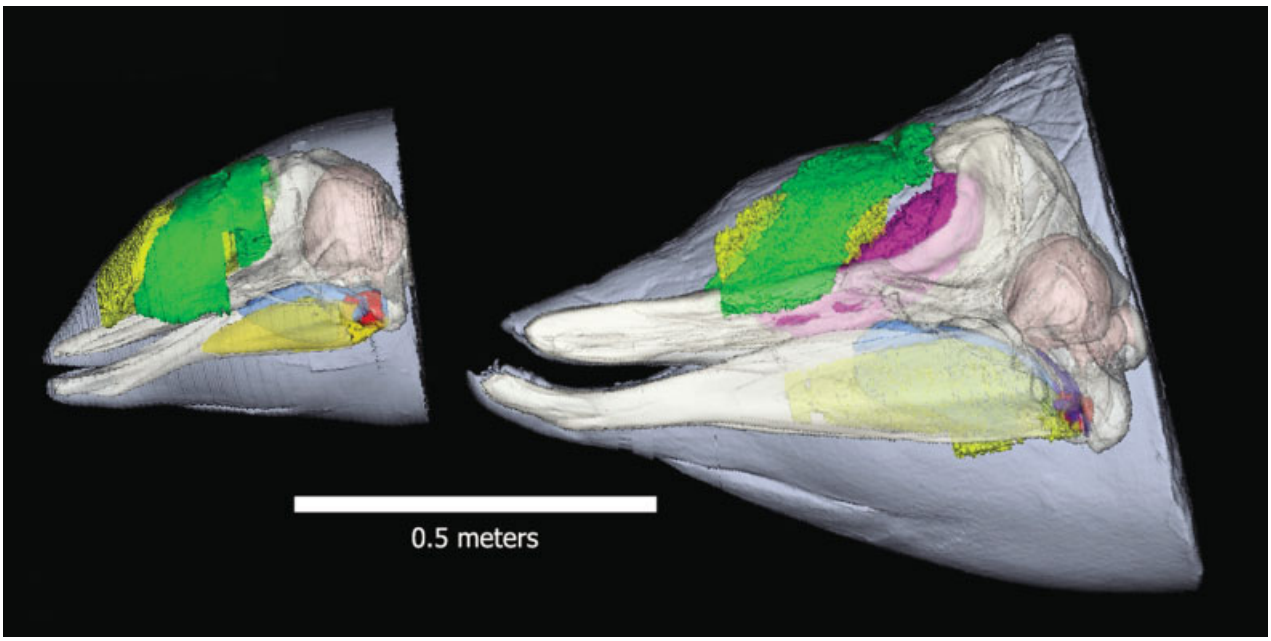

Fig. 2. Left lateral views of segmented heads of the neonate female and adult male Cuvier's beaked whales. The segmented structures are indicated by different colors: skin, light blue; melon and mandibular fat body, yellow; dense connective tissue theca, green; spermaceti organ, magenta; pterygoid sinus and peribullary sinuses, blue; tympanoperiotic complex, red; skull, white; brain, pink.

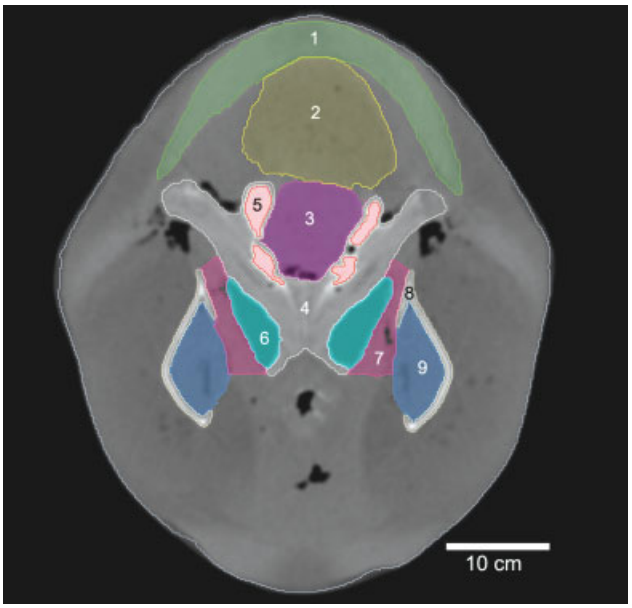

Fig. 3. Slice #271, a 1.5-mm section from the middle of the head in the adult male. It shows the segmented boundaries of various structures shaded and numbered (bilateral structures only numbered on one side). Moving from dorsal to ventral the outlined structures are (1) connective tissue theca (green); (2) melon (yellow); (3) anterior spermaceti organ (magenta); (4) skull (gray); (5) high-density premaxillary, maxillary, and vomerine components of the skull (red); (6) pterygoid sinuses (cyan); (7) fibrous venous plexus (magenta); (8) mandibles (gray); (9) mandibular fat bodies (blue); all enclosed within the boundary of the head.

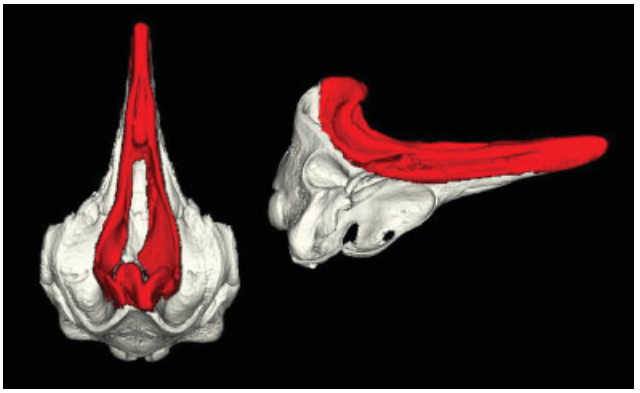

Fig. 4. This image set was produced by using a threshold algorithm to generate a new "object" of high-density bone and then overlaying it upon the skull. The figures make it easy to see the relationship between the high-density bones (red) collectively and the rest of the skull (ivory).

pact bone (Madar, 1998), resulting in higher density. These bones of the face could not achieve the extreme densities (2.25 g/cc) we have measured (see Table 1) without the addition of compact bone, and we therefore conclude that the condition is pachyosteosclerotic. The collective shape and position of these high-density bones are illustrated in Figure 4. In these views of the skull, the pachyosteosclerotic elements are colored red. These are the same bones that experience the greatest displacement and/or elongation in the process called "telescoping" (Miller, 1923). They are also the same bones

TABLE 1. Quantitative tabulation of volumetric and mean density values for various structures in the heads of an adult male and a neonate female Cuvier's beaked whale (*Ziphius cavirostris*), plus measurements for size indexing[a]

Specimen	Structure	Density (g/cc)	Volume (Liters)	Specimen	Structure	Density (g/cc)	Volume (Liters)	Neo/Adult % Vol
Zica Adult M	Anterior Spermaceti	0.84	2.899	Zica Neo F	Right Dorsal Bursa	1.03	0.0035	0.10%
Zica Adult M	Melon	0.87	2.345	Zica Neo F	Melon	0.96	2.120	40.43%
Zica Adult M	High-Density Facial Bones	2.25	2.882					
Zica Adult M	Skull	1.30	15.472	Zica Neo F	Skull	1.29	3.417	18.62%
Zica Adult M	Tympanoperiotic Complex (ear) Left	1.94	0.043	Zica Neo F	Tympanoperiotic Complex (ear) Left	2.01	0.054	126.08%
Zica Adult M	Tympanoperiotic Complex (ear) Right	1.84	0.041	Zica Neo F	Tympanoperiotic Complex (ear) Right	2.06	0.056	136.35%
Zica Adult M	Mandibles	1.37	2.078	Zica Neo F	Mandibles	1.28	0.424	20.39%
Zica Adult M	Pterygoid Sinus Left	−0.05	1.473	Zica Neo F	Pterygoid Sinus Left	0.34	0.391	26.55%
Zica Adult M	Pterygoid Sinus Right	−0.06	1.515	Zica Neo F	Pterygoid Sinus Right	0.36	0.439	29.00%
Zica Adult M	Mandibular Fat Body Left	0.82	1.853	Zica Neo F	Mandibular Fat Body Left	0.96	0.337	18.17%
Zica Adult M	Mandibular Fat Body Right	0.82	1.936	Zica Neo F	Mandibular Fat Body Right	0.94	0.334	17.27%
Zica Adult M	Brain	0.84	2.804	Zica Neo F	Brain	1.01	1.737	61.93%
Zica Adult M	Hyoids	1.08	0.796	Zica Neo F	Hyoids	1.21	0.134	16.87%
Zica Adult M	Connective Tissue Theca	1.00	2.557	Zica Neo F	Connective Tissue Theca	1.06	1.101	43.07%
Zica Adult M	All Combined	0.99	142.338	Zica Neo F	All Combined	1.00	32.721	22.99%

Specimen	Total Body Length (TL)	Condylobasal Length (SL)	Postcranial Body Length (PCBL)	PCBL/TL
Zica Adult M	515 cm	82 cm	433 cm	84.0%
Zica Neo F	315 cm	51 cm	264 cm	83.8%
Neo/Adult %	315/515 = 61%	51/82 = 62%	264/433 = 61%	

[a]Comparisons of volume and average density for structures within the heads of an adult male (Zica Adult M) and a neonate female (Zica Neo F). The large lipid fat body termed "anterior spermaceti" in the adult male is homologous to a small fatty region in the neonate female, similar to the right posterior dorsal bursa reported in dolphins (Cranford 1992). The adult male skull volume is equal to the volume of the high-density facial bones plus the volume of the rest of the skull (15.472 + 2.882 = 18.354) so that the ratio Neo/Adult % = (3.417/18.354 = 18.62%). There are no high-density bones in the face of the neonate, so that section of the table is blank. The bottom section of the table includes morphometric measurements of body length and condylobasal (skull) length so that an index of size (PCBL) can be calculated for comparative use with other fusiform cetaceans (See Cranford 1999).

that are in contact with the largest and lowest density lipid mass in the adult male forehead. This conspicuous low density fat body fills the prenarial basin and will be described in some detail below. We will refer to this structure as the "anterior spermaceti organ" (ASO[1]; Figs. 3, 6a–c, magenta color). This designation refers to the fact that this fat body is anterior to the main nasal passage, the spiracular cavity. This distinguishes it structurally, but perhaps not functionally, from the spermaceti organ found in sperm whales. In sperm whales, the spermaceti organ is posterior to the spiracular cavity (actually dorsal to it once the anatomic torsion in the head is taken into account), in contrast to the location of this specialized organ as we find it in *Ziphius* (Cranford et al., 1996; Cranford, 1999).

The anterior-most tip of the prenarial basin, formed primarily by the vomer and premaxillary bones, contain the highest density values (maximum CT# 22,490 = 2.87 g/cm^3), greater than any part of the bony (tympanoperiotic) ear complexes (maximum CT# 22,163 = 2.82 g/cm^3), which are generally thought to be the densest bones in cetaceans (Kasuya, 1973). The consequence of this construction is a very abrupt density change at the interface between the tip of the large ventral fat body (ASO) and the high-density facial bones that comprise the rostral cavity. The density difference between the fat body and the high-density facial bones is apparently the greatest that can be achieved between two adjacent tissues. The difference between the mean density of the premaxillary bones (18,217 CT# = 2.25 g/cm^3) and the mean density of the large fat body (ASO) in the adult (8513 CT# = 0.83 g/cm^3) accounts for some 50% of the density variation across the entire specimen. The maximum range of density values across the entire specimen (2833 CT# - 22,516 CT# = 0.00 g/cm^3 – 2.87 g/cm^3) is wider than that for all "tissues" because it includes air spaces, which are not tissues, and some debris (i.e., sand) that accumulates in the mouth and nasal cavities during the process of stranding, dying, and the carcass rolling around on the beach.

The skeleton of any neonate mammal is largely cartilaginous, and our neonate *Ziphius* is no exception. Scans of the neonate showed no evidence of high-density centers of ossification.

If we compare the fat bodies in the foreheads of the neonate and the adult (Fig. 5), we see that both heads contain masses of fat that ride atop the skull. Their relative volumes are listed in Table 1. In combination, the fat bodies extend from the phonic lips, underneath the overhanging vertex of the skull (Fig. 5a), to a point approximately halfway along the anterior portion of the bony rostrum. The dorsal-most fat body is the melon. It is in the same relative position (i.e., homologous) in all extant odontocetes (yellow structure in Figs. 5–7; McKenna, 2005). The position and geometric relationships between these fat bodies are shown in Figures 5–7, tabulated in Table 1, and described in detail below. The density difference between them is slight but consistent and presented in Table 1.

The primary difference in these two fat bodies is that, in the adult male, the low density fat body (ASO) projects ventrally into the prenarial basin (Fig. 5a). Distinguishing between these lipid and connective tissue structures (melon and anterior spermaceti organ) is based primarily upon position and geometry but also on density differences and distinctive appearance during dissection of the adult male.

In contrast to the melon, the ASO appears to be a specialized organ in the adult male *Ziphius* (Norris and Harvey, 1972). Distinctly separate, the ASO is rounded in cross-section and bounded by dense bony elements laterally and ventrally. The lipid tissue of the ASO is also visually distinctive. It is pearlescent white and somewhat pellucid, unlike the adjacent melon. The ASO contains fibers that appear more fine than those in the melon and they appear to be oriented primarily anteroposteriorly.

The image sequence in Figure 6 isolates the skull (white) from the melon (yellow) and anterior spermaceti organ (magenta). The melon is located atop the bony rostrum and anterior to the main (spiracular) nasal passage, where we expect to find the melon in other odontocetes. It is also more or less fusiform in shape, like other odontocete melons.

The anterior spermaceti organ is the largest fat body (by volume) in the forehead of the adult male *Ziphius*, located just ventral to the melon and nestled within the high-density bony cradle of the facial region, the prenarial basin described above. The term "spermaceti organ" is normally reserved for the hypertrophied lipid structure in the sperm whale (Mead, 1975; Cranford, 1999). But there is evidence that the spermaceti organ probably has a homologue in every extant odontocete species (Cranford et al., 1996).

Norris and Harvey (1972) first suggested that the large fat body, which fills the prenarial basin in the adult male *Ziphius*, might be homologous to the spermaceti organ in the sperm whale. This is an intriguing notion that will be discussed later in this report. We conditionally accept Norris and Harvey's (1972) terminology for the purposes of reporting the remainder of the results but remain skeptical of their suggestion that the two structures are homologous. The primary reason for this skepticism is that, during our dissections, it appeared that the fat body in question (magenta structure in Figures 5–7) was not positioned posterior to the main nasal passage, also called the spiracular cavity. We believe that the two low density fatty structures may be functionally equivalent and, as a consequence, we will retain Norris and Harvey's term with the condition that we make clear the anatomic distinction. As a result, we adopt the term "anterior spermaceti organ" to denote that it is anatomically distinct, while maintaining the original term to denote the potential analogous functional connection. The details of the anatomic evidence for and against this notion will be reviewed in the Discussion section.

It is interesting to note that the configuration of the two fat bodies in the adult male *Ziphius* resembles the arrangement of the spermaceti organ and the junk in a sperm whale's head, except that the *Ziphius* anatomy is upside down from that of the sperm whale.

The ventral surface of the anterior spermaceti organ in *Ziphius* is reminiscent of the sweeping curvature of a "cesta," the wicker basket made to catch and throw the ball in Jai-Alai. The bones of the face in the male *Ziphius* and the Jai-Alai basket both form a concave channel that deepens into a smooth pocket at the base of the curve. This is illustrated in Figure 6a, the first

[1]See note 4, page 8 in *Nomina Anatomica Veterinaria* (1994). Ithaca, New York, International Committees on Veterinary Gross Anatomical Nomenclature, Veterinary Histological Nomenclature, and Veterinary Embryological Nomenclature.

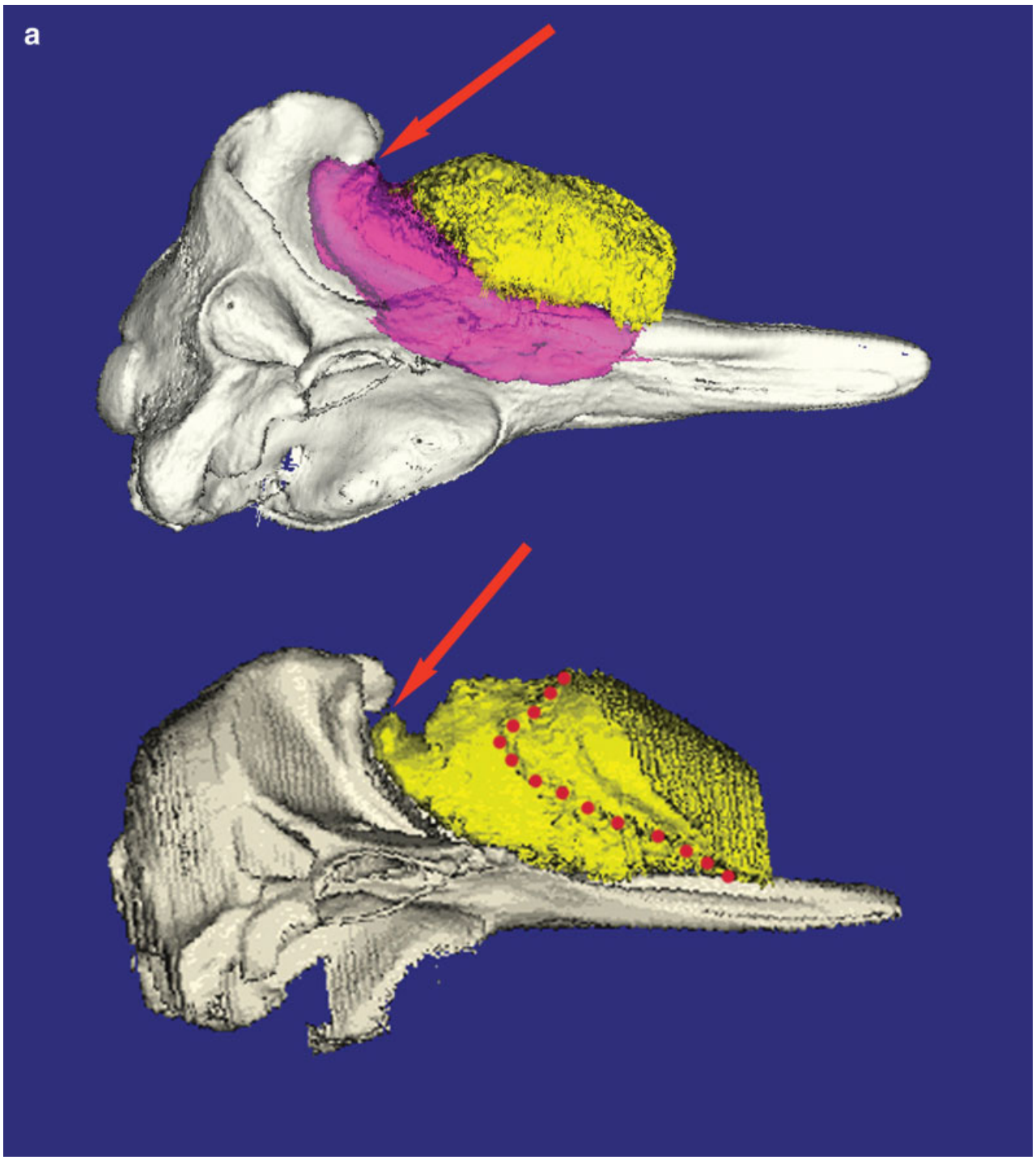

Fig. 5. **a:** Right lateral views of forehead fat bodies in the adult male (top) and the neonate female (bottom). The image of the neonate has been scaled up to approximate the size of the adult so that shape comparisons of the forehead fat bodies can be made. A dotted red line, on the neonate divides the melon into two components drawn according to where the melon narrows posteriorly. The similarities in shape and position between the forehead fat bodies in the adult male and neonate female specimen suggest homology. Red arrows indicated location of right phonic lips. **b:** Dorsal view comparison of forehead fat bodies in the adult male (top) and the neonate female (bottom). The image of the neonate has been scaled up to approximate the size of the adult so that shape comparisons of the forehead fat bodies can be made. A dotted red line on the neonate divides the melon into two components drawn according to where the melon narrows posteriorly.

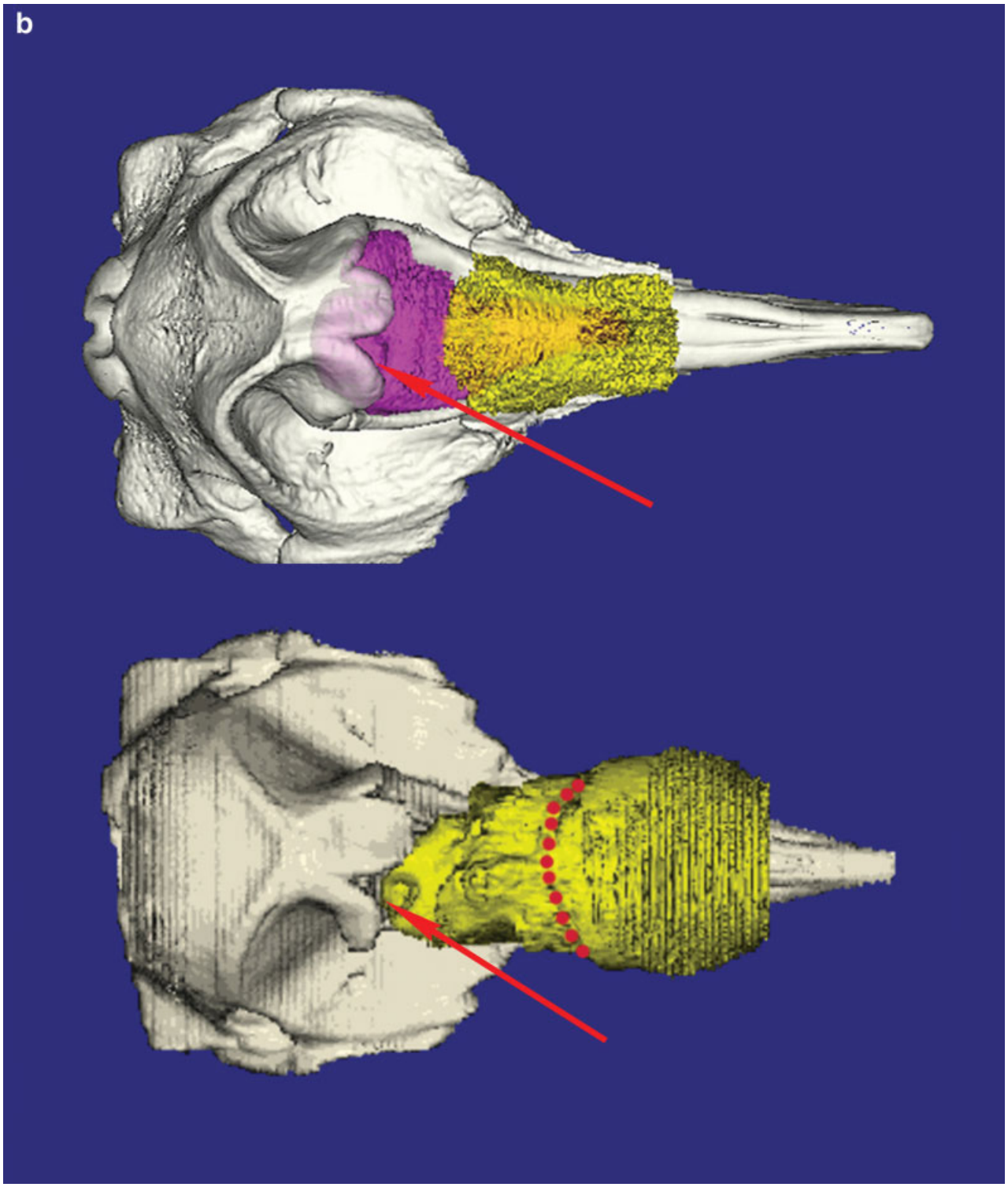

Figure 5. (continued)

image in a composition of six right lateral views of the skull, lipid components, and the connective theca in the adult male *Ziphius*.

During dissection, we made a series of transverse cuts across the forehead of both specimens. This method is similar to the technique used by Green et al. (1980) for bottlenose dolphins. In the adult male, the melon appears ovoid in cross-section and light pink to white in color. Families of parallel connective tissue fibers run horizontally across the cut surface of the melon in each

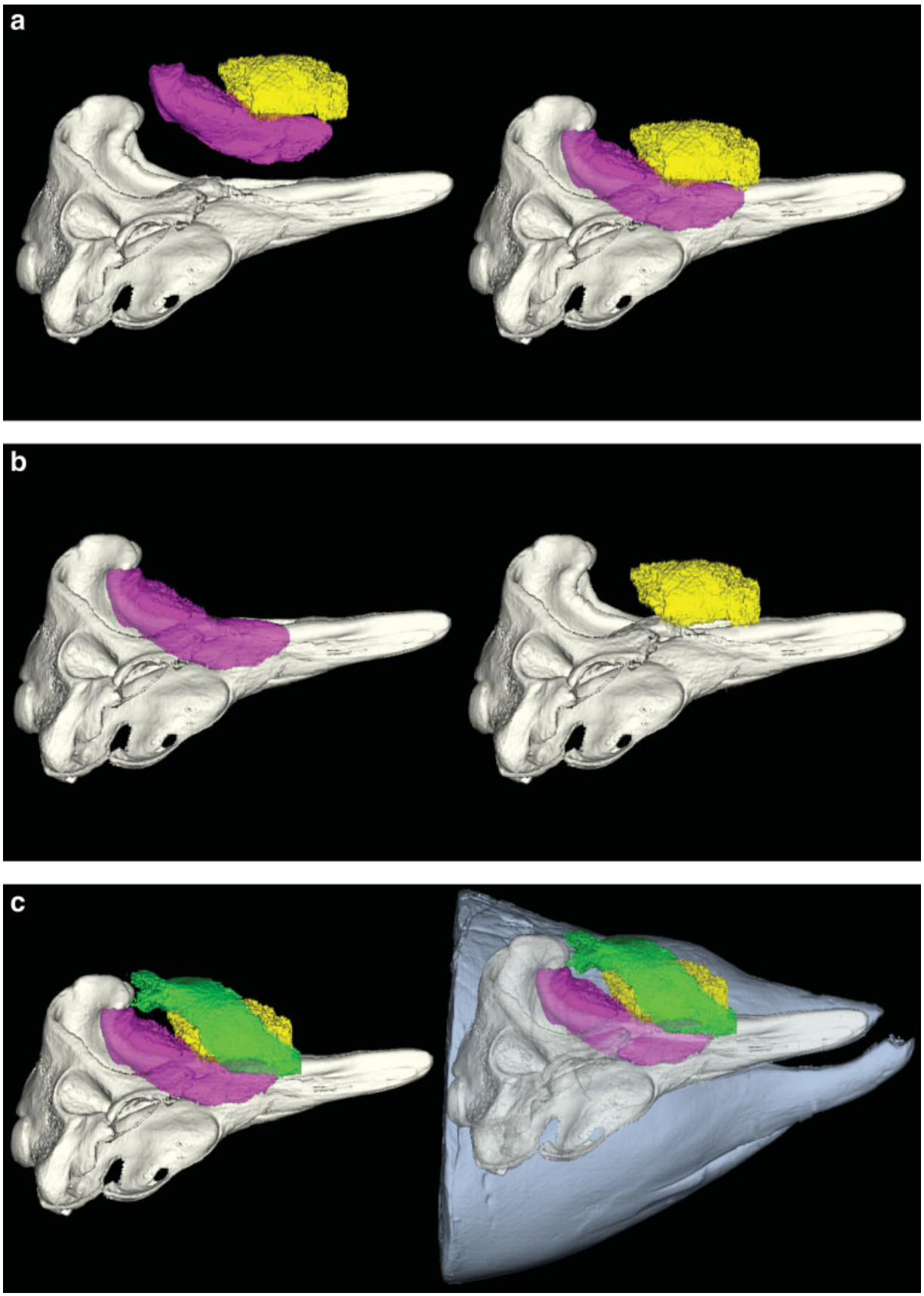

Figure 6.

section. These horizontal fibers appear to be connected to the rostral muscles that buttress the lateral margins of the melon. Some fibers also run anteroposteriorly but few if any fibers appear to be oriented dorsoventrally. Each section is capped by the dense connective tissue theca, which, in the adult, is consistently at least 4 cm thick (Fig. 3) and is composed of fibers that appear to be oriented in all directions.

We made similar transverse sections across the melon in the head of the neonate specimen. The characteristics were visually very similar except that the central core of the melon did not have the pellucid characteristic and the fibers did not appear to be as well developed in diameter or number. This finding suggests a pattern similar to that reported by Koopman and her colleagues, where neonates do not have a full complement (in specie or volume) of the fatty molecules of adult odontocetes (Koopman et al., 2006; Zahorodny, 2007).

The band of connective tissue that arches over the fat bodies of the forehead (Fig. 6c) is anchored to the vertex and the maxilla, and is well developed in beaked whales. This connective tissue arch is likely homologous to the structure that has been previously referred to as the "connective tissue theca" in other odontocetes (Cranford et al., 1996). It does not encase the entire posterior extent of the fat bodies in *Ziphius*, as this is accomplished by the pachyosteosclerotic bones of the face. This "theca" is clearly visible as an arch of dense connective tissue (Fig. 6c).

The context of this dense connective tissue arch (green) and the skin (blue) can be seen in Figure 6c; it shows all of the major forehead components together (excluding muscles). It is clear from this composition that the melon projects out through the connective tissue arch and is directed anteriorly or forward, suggesting a pathway for sound transmission that is similar to those known for well-studied odontocetes.

Figure 7 shows the same set of component structures as in Figure 6 but from a dorsal view. The perspectives in Figures 6 and 7 are perpendicular and provide a means for the reader to understand the complete 3D geometry of the forehead anatomy in the adult male *Ziphius*. This figure shows the relationship of skull to both primary fat bodies, the arching dense connective tissue theca, all within the bounds of the head.

Note that the posterodorsal most aspect of the anterior spermaceti organ is where we find the phonic lips (Cranford, 1999), formerly known as the "monkey lips" or "monkey muzzle" (Pouchet and Beauregard, 1885). Figure 8 shows a photograph of the phonic lips from the dissection of the adult male. The location of the right phonic lips is shown by the red arrow in the upper panel of Figure 5a.

We report quantitative volumetric fractions and average density values for various structures within the heads of the adult and neonate specimens in Table 1. We measured volumes for the structures of interest, primarily those suspected of a significant role in acoustic function. Table 1 includes measurements for the skull, melon, anterior spermaceti organ (or its homologue), ears, mandibular fat bodies, and pterygoid sinuses, as well as a few linear measurements for total body length, linear distance between the ears, and condylobasal length of the skull. All of these measurements were taken from the CT scans of our two *Ziphius* specimens.

We use the total body length (TL) and condylobasal length or "skull length" (SL), from which to calculate an index called postcranial body length (PCBL; as described by Cranford, 1999). This index was constructed to exclude the influence of differences in the feeding apparatus on body size comparison. The evolution of the feeding apparatus has had a significant affect on the morphology of odontocete cephalic anatomy. For example consider the elongate jaws of platanistoids compared with the shorter and wider jaws of modern delphinoids. The PCBL index removes any inordinate contribution of skull length to estimates and comparisons of body size. Because all cetaceans have fusiform body shapes (Silva, 1998), the PCBL can be used as an index of relative size for quantitative (volumetric) comparisons of homologous anatomic structures across groups of odontocetes. This method is not particularly useful for comparisons within the same species, as is evident by the values at the bottom of Table 1. However, these values could be useful to future investigators attempting to make geometric comparisons across the suborder, so we include them in Table 1.

Sound reception anatomy of the basicranium and gular region. The anatomy on the ventral aspect of the head is morphologically complex, suggesting functional significance. This report focuses on the anatomy of the hearing apparatus and its accessory structures. All odontocetes have the same basic form in the hearing apparatus (Fig. 9). There are several structures that bear directly upon our understanding of the sound propagation pathways and the potential effects of deep diving on hearing.

We will concentrate on describing the anatomic geometry of the conventional acoustic pathway into the head. One proposed pathway begins with a fatty pad, the "acoustic window" (Norris, 1968), which lies external to the thinned lateral wall of the posterior expansion of each mandible, often referred to as the "pan bone." The mandibles in odontocetes are hollowed out, lack a medial bony lamina opposing the pan bone, and contain the

Fig. 6. **a:** Zica Adult M. The first image of the set shows the skull and the two primary fat bodies of the forehead, the melon (yellow), and the anterior spermaceti organ (magenta). In the left panel, the fat bodies have been separated from the skull, for the purposes of this illustration, but maintain their proper relationship to one another. In this image, we see the sweeping curvature of the ventral surface of the anterior spermaceti organ (colored magenta), which matches the curvature of the channel in the skull formed by the prenarial basin and the face of the skull that then rises up to the overhanging vertex posteriorly. The right panel shows the two fat bodies in their correct relationship to the skull. The skull has been made slightly transparent in these images to illustrate that the lower lipid body is largely embraced or encased (except along the dorsal surface) by skull bones. **b:** This panel shows each of the two fat bodies of the forehead separately in their correct geometric relationship to the skull. **c:** This panel shows all of the major forehead components together (except muscles), skull, anterior spermaceti organ, melon, and an overarching cap of dense connective tissue (green), plus the skin (blue).

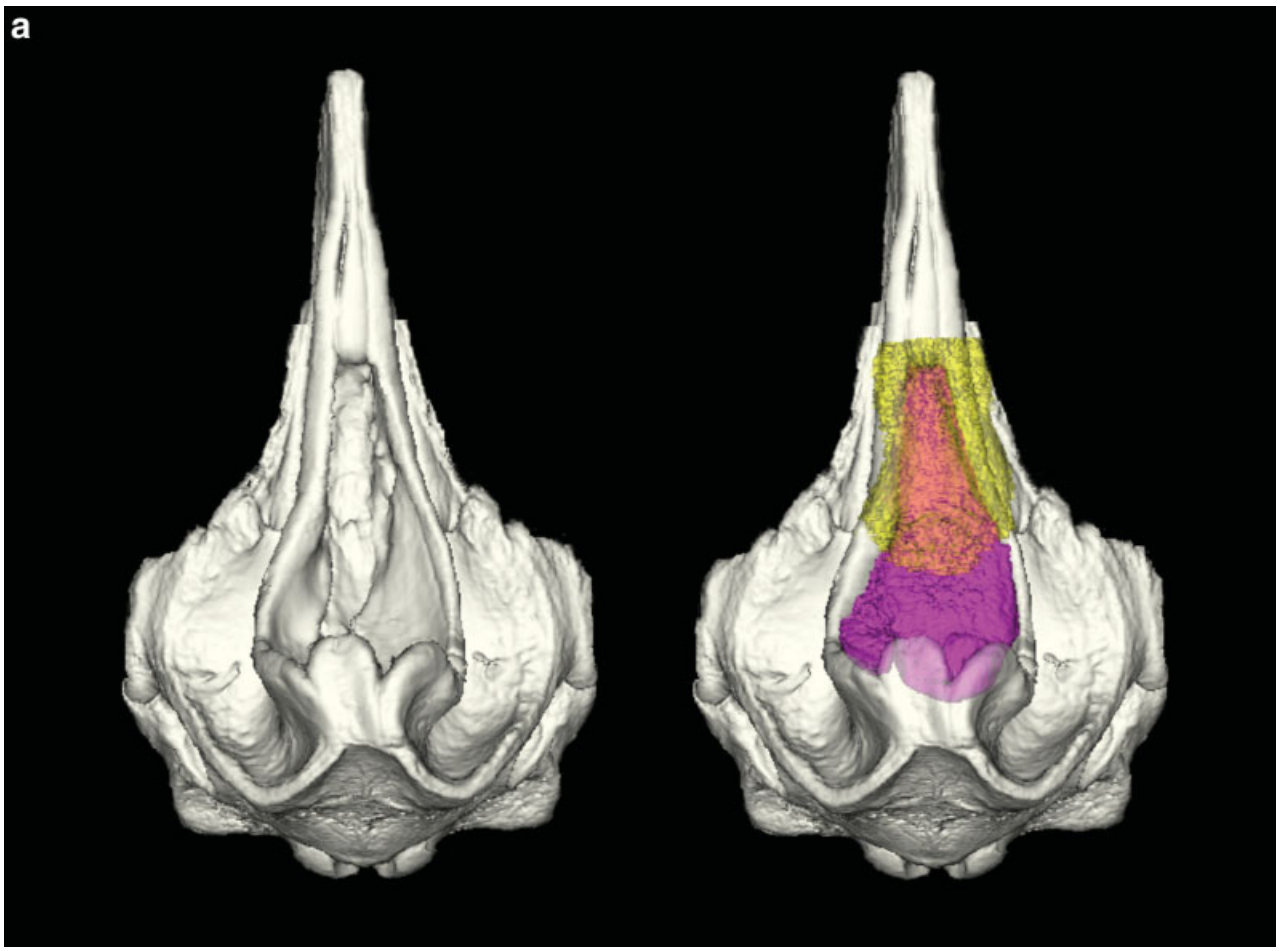

Fig. 7. **a:** This panel shows the dorsal view of the skull on the left and the skull with both primary fat bodies on the right. In this dorsal view, posterior is toward the bottom of the image. As in other odontocetes, the midline of the skull is skewed to the left and is the result of the hypertrophy of the soft tissue anatomy on the right side of the forehead. **b:** These images show the fat bodies isolated with the skull in each case to emphasize their distinct boundaries. Note that the anterior spermaceti organ narrows anteriorly and ends at the anterior tip of the prenarial basin where we also find the highest density bones in the head. **c:** The dense connective tissue arch (purple) is the most prominent structure in this panel. The horizontal dark cleft near the posterior aspect of this arch is indicative of the blowhole.

internal mandibular fat bodies (MFB; Fig. 9). The internal MFB connect to the bony ear complexes posteriorly and are the most likely conduits for sound to the ears (Norris, 1964, 1968, 1969). The structure of the MFB is not homogeneous, and the complex topography needs further study (Ackman et al., 1971, 1973; Litchfield et al., 1975, 1976; Koopman et al., 2006; Zahorodny, 2007).

The internal MFB narrows posteriorly, gives off two branches, and abuts the tympanoperiotic complex in exactly two locations (Fig. 11). The largest (ventral) branch attaches along the ventrolateral aspect of the tympanic bulla, as noted by Norris (Norris, 1964, 1968, 1980; Norris and Harvey, 1974). In addition, there is a second, smaller branch of the MFB, which runs dorsally and attaches to the tympanoperiotic complex in a furrow or sulcus just anterior to the sigmoid process (Fig. 11). The ramifications of this finding will be described and discussed elsewhere (Cranford and Amundin, manuscript in preparation).

The pterygoid sinuses are perhaps the most prominent components of the structures associated with the hearing apparatus (Figs. 3, 9, 13, 14). They are paired structures, bounded medially by an elongate depression in the skull (the pterygoid bone), and laterally by the FVP. The pterygoid sinuses in beaked whales (Ziphiidae) and the sperm whales (Physeteridae) are proportionately much larger than in other odontocetes (Fraser and Purves, 1960). The pterygoid bone has no outer lamina, which allows the membranous lateral wall of the sinus to expand, greatly increasing the potential volume of the pterygoid sinus.

Each pterygoid sinus fits into a depression in the skull that runs posteriorly along the ventrolateral skull, from a point anterior to the widest part of the skull (Figs. 5, 6, and 10). Both pterygoid sinuses ramify posteriorly into a series of projections, known collectively as the peribullary sinuses, which form an acoustic shield along the posteromedial aspect of the each bony ear complex (Figs. 13, 14). The juxtaposition of the extensive air sinus system to portions of the lipid sound conduction pathway and the bony hearing organ makes this area an obvious focus for investigation, modeling, and simulation.

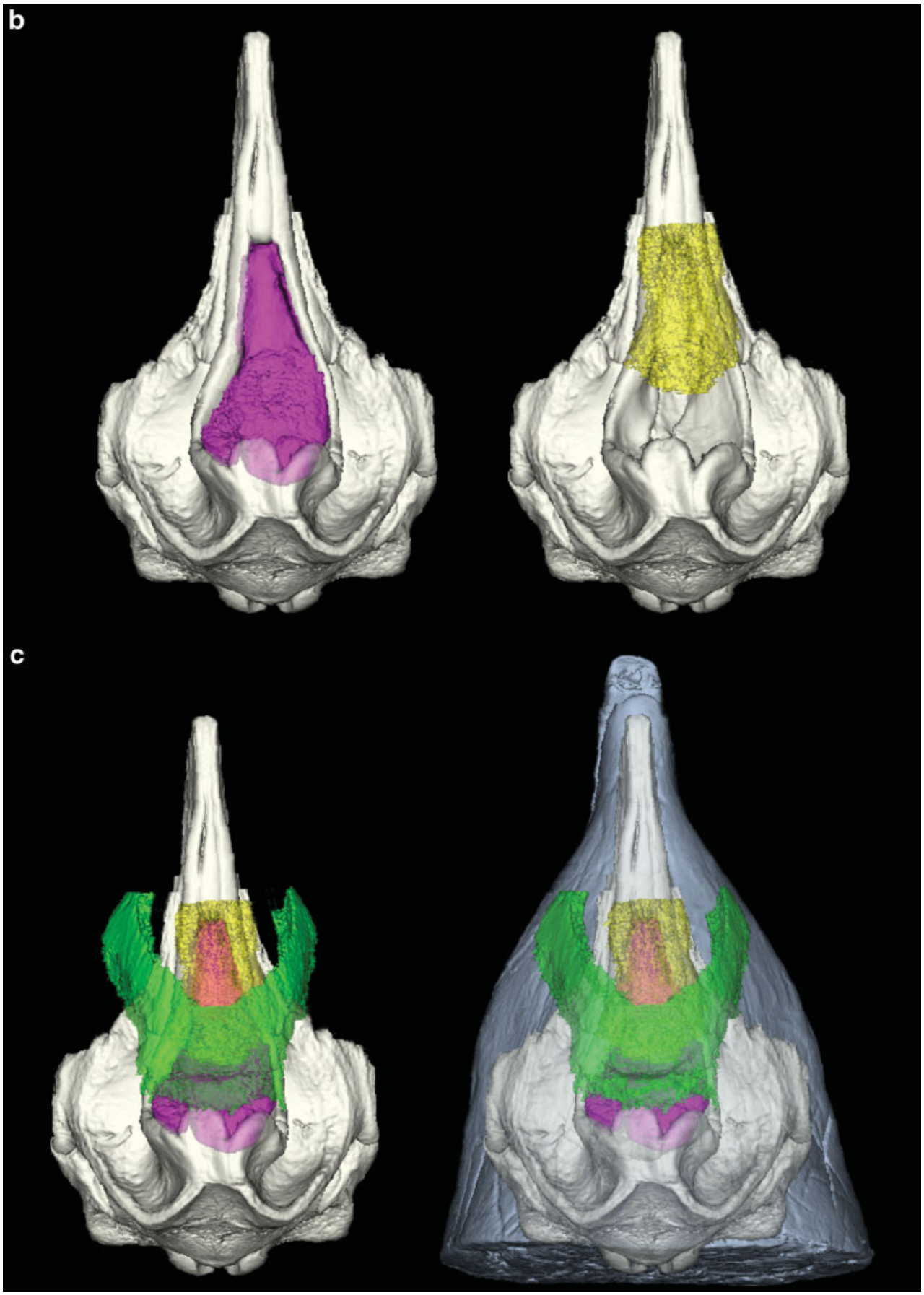

Figure 7. (continued)

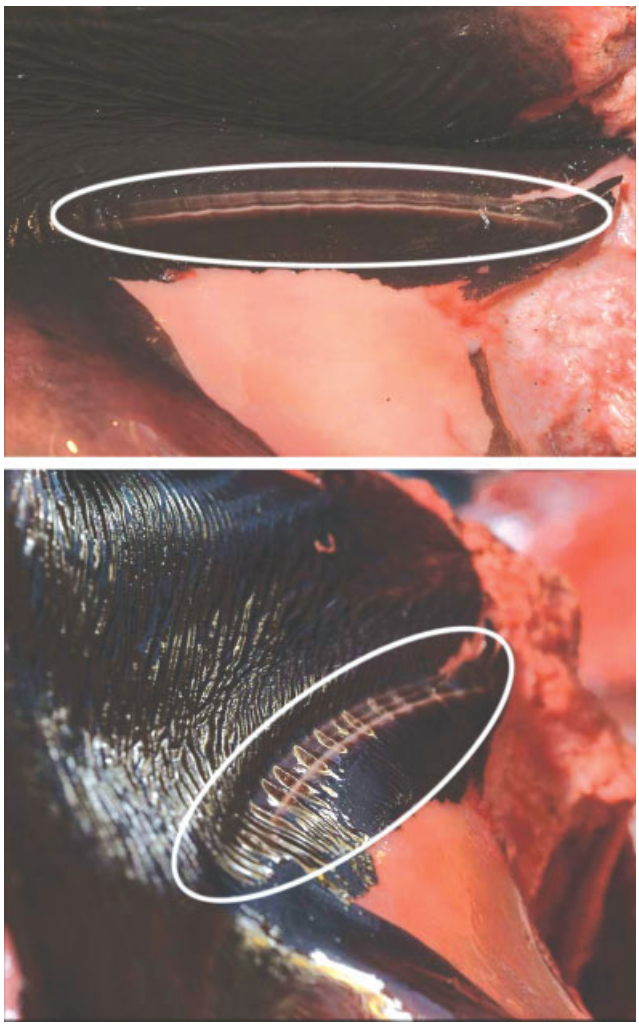

Fig. 8. The right anterior phonic lip of an adult male Cuvier's beaked whale shown from two angles. The upper panel shows a plan view of the lip indicated by a series of light parallel bands across the field enclosed by the white oval. In the lower panel shows a dorsomedial view of the same lip. The axis of the lip is indicated by the light gray line that travels along an axis that is parallel to the white oval. The view also shows a series of ridges that are perpendicular to the axis of the lip. These ridges are prominent because the tension on the lips has been relaxed during the dissection. These ridges and grooves are common to all odontocete phonic lips examined to date. They may play a role in directing the flow of air during the sound generation process. The phonic lips are likely the site of sonar signal generation.

In general, the FVP lies between the pterygoid sinuses and the MFB (Figs. 3, 9, 11, 12). Each venous plexus can be engorged with blood, causing its medial membrane to expand and occlude the adjacent pterygoid sinus (Fraser and Purves, 1960). Throughout its anterior two thirds, the gossamer-like trabecular structure (Fig. 12) is sandwiched between its medial and lateral membranes. The anterior FVP appears capable of extraordinary distensibility into the pterygoid sinuses. The character of the FVP changes rapidly along the posterior third so that the connective tissue walls are much thicker and the blood-space much smaller by comparison. Consequently, the potential distensibility in the

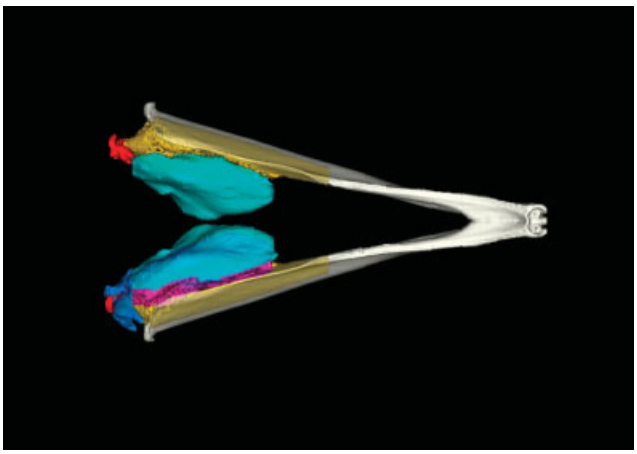

Fig. 9. Dorsal view of the hearing apparatus from the adult male Cuvier's beaked whale (*Ziphius cavirostris*). Displayed are the mandibles (white), the mandibular fat bodies (gold), the pterygoid sinuses (green), the fibrous venous plexus (magenta), the peribullary sinuses (blue), and the bony ear complexes (red). For demonstration purposes, the fibrous venous plexus (FVP) is seen sandwiched between the mandibular fat body and the pterygoid sinus on the right side but turned off on the left. The peribullary sinuses (blue) are not illuminated on the left side to reveal the relationship between the mandibular fat body and the bony ear complex. The external mandibular fat bodies are not pictured.

posterior third of the FVP is greatly reduced. It is this posterior third of the FVP that is adjacent to the peribullary sinuses and the bony ear complexes (Fig. 11).

The primary component of the hearing apparatus is the organ of transduction, the dense bony ear (tympanoperiotic) complexes. As the term suggests, each tympanoperiotic complex (TPC) is a functional and structural unit composed of a fusion between the tympanic and periotic bones. Its structure is complicated and has been the source of considerable study (Wever et al., 1971; Kasuya, 1973; Fleischer, 1976, 1980b; Ridgway, 1999; Ketten, 2000). We will not describe it in any detail here, but the structure of the tympanoperiotic complexes will be described using a comparative approach in a subsequent paper (Cranford and Amundin, manuscript in preparation).

Estimates of Error and Bias

The results tabulated in Table 2 give us some sense of the variation contained in our quantitative measurements. All of the numbers in Table 2 were obtained from segmenting the tympanoperiotic region in the adult male specimen used in this study. It compares the computer-only threshold technique at various density ranges with the abilities of experienced human observers using various image processing tools. Generally, the threshold technique should provide the most consistent results because it is relatively easy to use if the tissues structures have dramatic density differences along their boundaries, as in the case around the bony ear complexes. The tympanoperiotic region of the adult male *Ziphius* was scanned twice using different slice thicknesses (see the Methods and Materials section). Both sets of data were used in the compilation of Table 2, as designated in the column labeled "Scan Thickness." A few generalizations can be

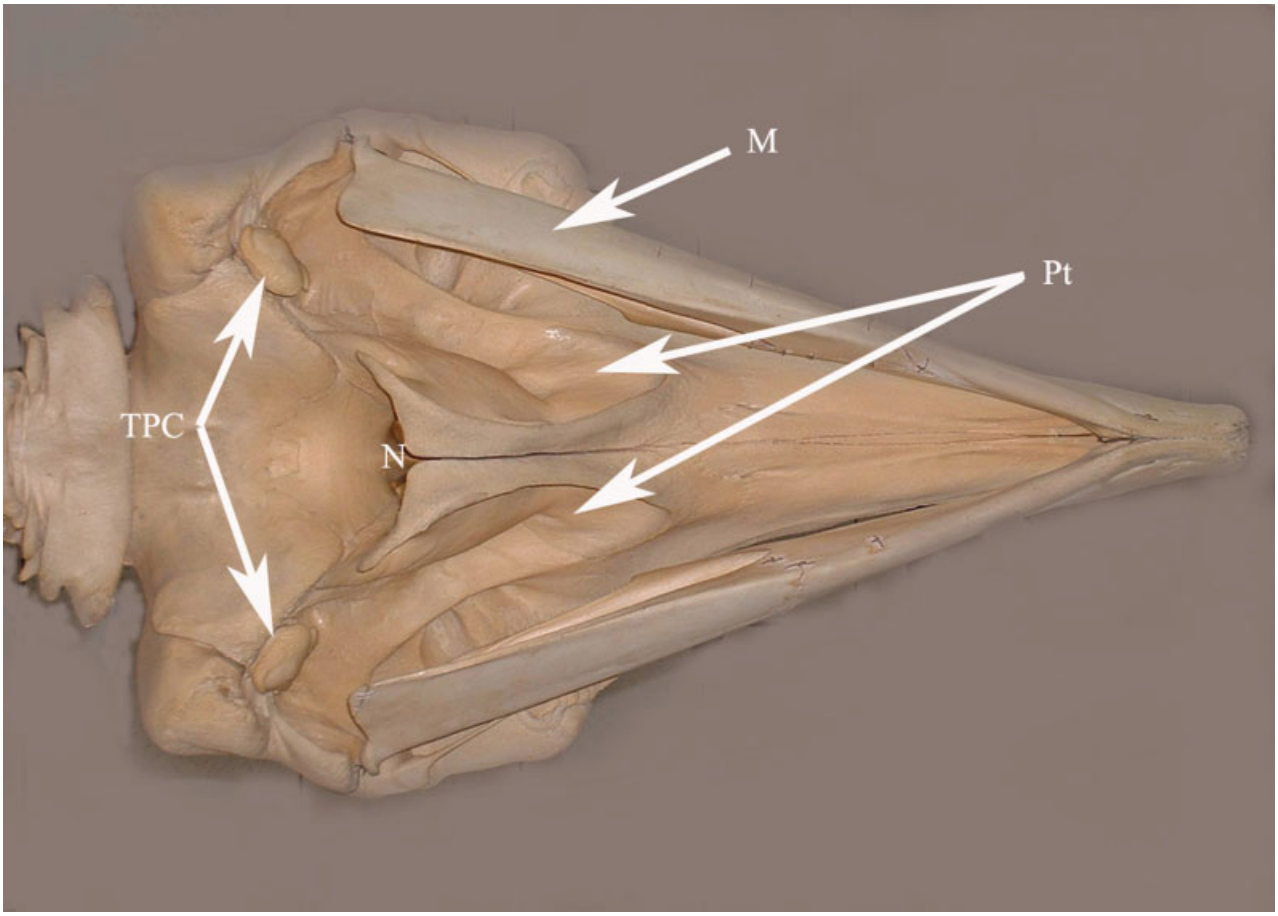

Fig. 10. Ventral view of the skull and mandibles in an adult male *Ziphius*. Visible are the tympanoperiotic complexes (TPC), the bony nasal passages (N), the mandibles (M), and the depressions in the pterygoid bones (Pt) of the skull to which the pterygoid sinuses are attached. (This specimen is on display at the San Diego Museum of Natural History.)

gleaned from Table 2 by comparing two techniques. The first technique uses a threshold range and relies solely on computer tools (Table 2, rows 1–6). The second technique combines human decision-making skills with image processing tools (Table 2, rows 7–10).

As expected, segmentation based solely on thresholds show that the wider the threshold range (rows 2–5), the greater the volume captured, simply because widening the range includes more voxels. In rows 1 and 2, the threshold (density) range is equal but the slice thickness of the tomograms are different (1.5 vs. 0.6 mm), resulting in measured volumes that are different by approximately 5%. The tomograms used in row 1 are just over twice as thick as the scans used for row 2. Because the CT scan algorithm averages across the entire thickness of each slice; averaging over a thicker region should depress the upper part of the density range and therefore put more voxels within the chosen threshold range. So, even if we scan the same specimen in the same CT scanner, slightly different voxel values can be produced, depending upon the scanning protocol used. The implication here is that using different slice thicknesses during scanning can affect the voxel values to some degree. It is unlikely that the differences are due to interpolation in Analyze because the same cubic spline was used to produce both volumes.

It appears that small differences in voxel values can be attributed to different slice thicknesses. At the same time, we can be certain that large volumetric differences between structures in the neonate and the adult are real and indicate significant anatomic distinctions (Table 1).

To test the consistency of the calculations produced by the image processing software (Analyze 5.0), we calculated the same threshold range on the same data set multiple times (see Table 2, rows 3, 4). The volume difference is 0.04 cubic centimeters, a very small difference indeed.

Table 2 also allows us to compare measurements made by humans using computer tools vs. measurements based completely upon threshold values (computer only). The volumes measured using human decisions were within the range found using the purely threshold technique. Upon inspection, the results in Table 2 suggest that the widest threshold range (row 1) captured too many voxels (i.e., some that were not part of the structure) and the smallest threshold range (row 6) probably did not catch all of the voxels that should be counted as part of the ear complex (note that rows 1 and 6 used the same slice thickness). This finding inspires confidence that the human plus computer technique is the best. This is particularly apparent when we consider that the boun-

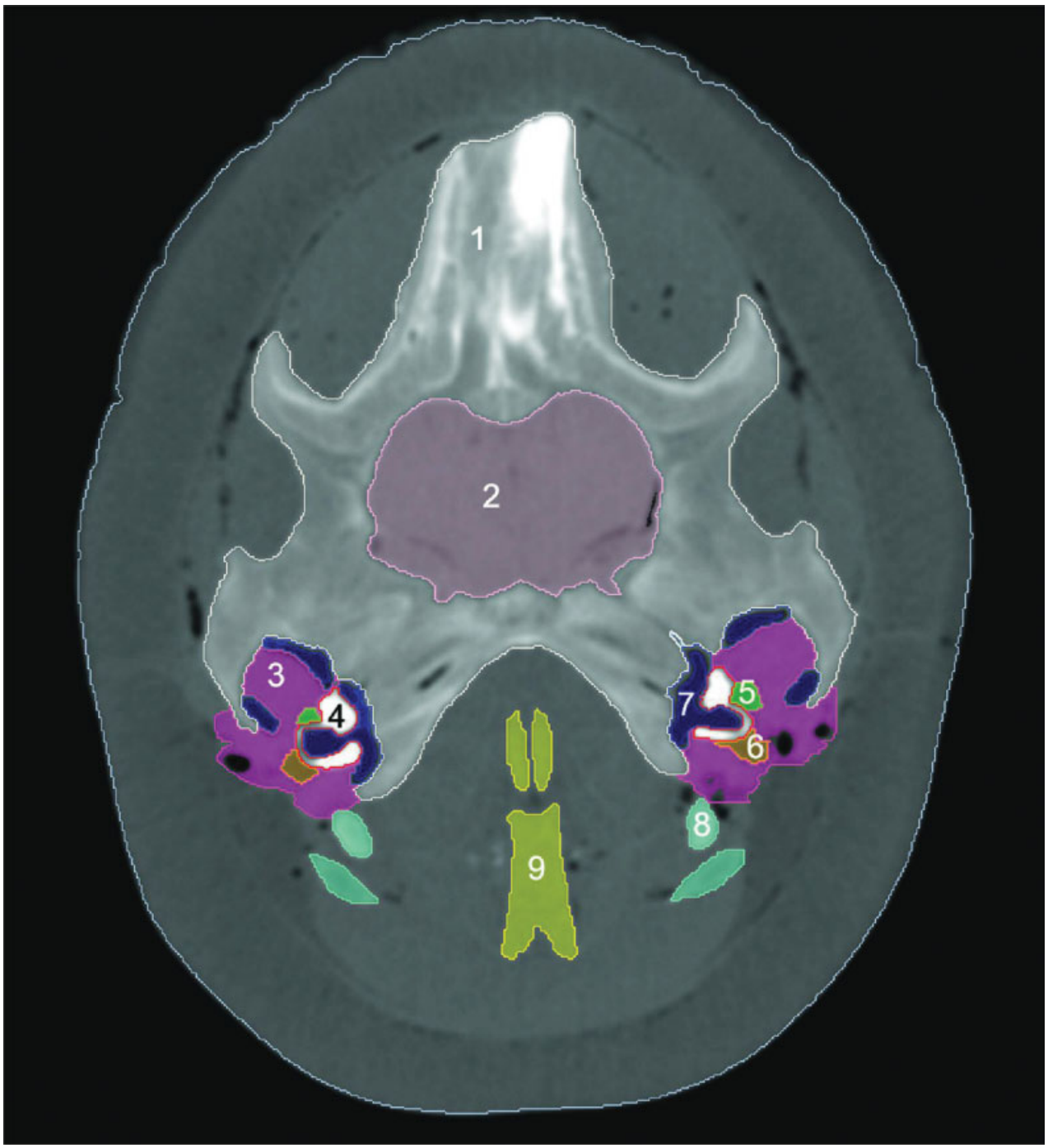

Fig. 11. Adult male Zc scan # 103, a 1.5-mm transverse section through the hearing apparatus. The segmented structures are bounded by colored lines and are numbered (bilateral structures are numbered only on one side): (1) skull (gray), (2) brain (pink), (3) fibrous venous plexus (magenta), (4) tympanoperiotic complexes (white), (5) dorsal branch of the mandibular fat bodies (green), (6) ventral branch of the mandibular fat bodies (orange), (7) peribullary sinuses (blue), (8) hyoid bones (turquoise), and (9) larynx (yellow), all contained within the skin.

daries of the ear complexes are relatively easy to segment using the threshold technique alone. Consequently, we can assume that as we move from easily defined boundaries to those that are more difficult to distinguish, the (computer only) threshold technique will be progressively worse at segmenting structural boundaries.

Rows 7 and 8 show measurements taken more than 2 years apart by the same operator (TC), row 9 used a different slice thicknesses. Row 10 shows the results from a different operator (M.M.). These data give us some sense that observer bias in trained individuals is not a cause for concern.

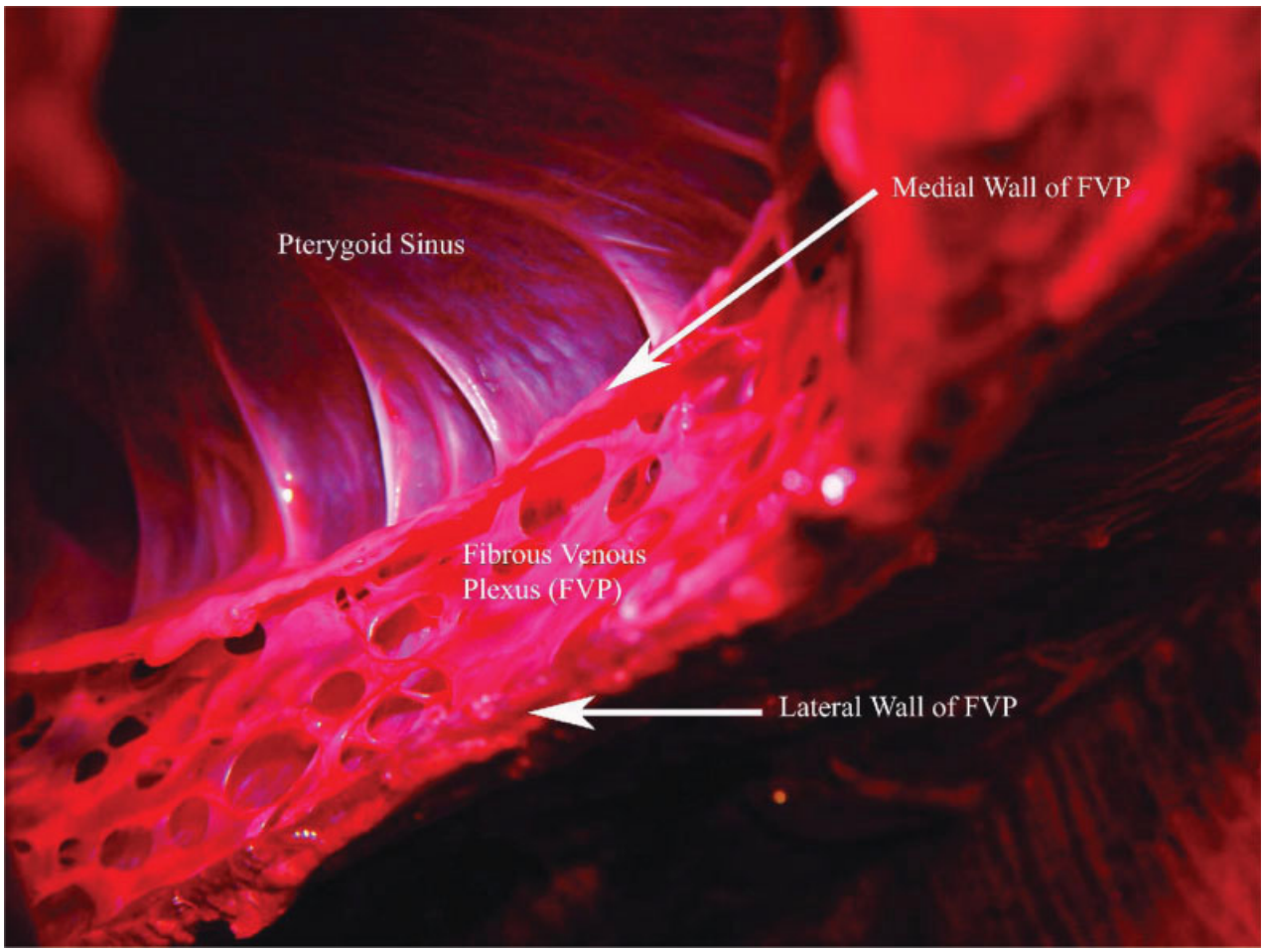

Fig. 12. Zica Neo F dissection showing the gossamer-like trabeculae of the anterior two-thirds of the fibrous venous plexus (FVP). The section cuts across the FVP so that it can be seen in the foreground.

DISCUSSION

Forehead Anatomy

The ASO (anterior spermaceti organ) is the most prominent and voluminous structure in the forehead of our adult male *Ziphius*. It occupies almost 3 liters (Table 1), filling the prenarial basin and extends posteriorly to the phonic lips, on either side of the nasal septum. The ASO apparently only occurs in this hypertrophied form in adult males. We have examined a few skulls of both adult male and adult female specimens of *Ziphius* in the collection at the Natural History Museum at the Smithsonian Institution.[1] By simple inspection, we see that females lack this bony basin and, by implication, the hypertrophied fat body that fits within it. At the same time, our neonate female shows that an extension of the fatty melon, perhaps a homologue of the ASO, does reach the right phonic lips (Fig. 5a,b). The osteological observations of the adults clearly indicate that the nasal anatomy within the "forehead" of *Ziphius* is sexually dimorphic.

Beyond this, it is not possible to extrapolate the anatomy of an adult female from a neonate to any meaningful degree. It is important to remember that this report is unfortunately based upon only two specimens. One reason that the knowledge base for this species is so depauperate is because it is difficult to obtain a representative number of specimens. Consequently, we would generally be unable to distinguish whether some of the comparative differences we see are related to age differences rather than gender differences. Immature specimens generally lack tissue differentiation and do not contain a complete array of lipid compounds (Koopman, 2007; Zahorodny, 2007); this may be why, for example, that in the neonate we were unable to clearly delineate the fat bodies homologous to the dorsal bursae in delphinoids (Cranford et al., 1996) and normally associated

[1]The reader can confirm this by comparing images of skulls online at an exquisite beaked whale Web site developed by the Smithsonian Institution: http://vertebrates.si.edu/mammals/beaked_whales/pages/main_menu.htm. A side by side comparison of the adult male and female skulls can be found at http://vertebrates.si.edu/mammals/beaked_whales/pages/zca/zca_ost_pg1.htm. The striking demonstration of sexual dimorphism in the nasal region of the skulls of adult Ziphius can be readily seen in the anterior views at http://vertebrates.si.edu/mammals/beaked_whales/pages/zca/zca_ost_pg5.htm and http://vertebrates.si.edu/mammals/beaked_whales/pages/zca/zca_ost_ pg6.htm.

TABLE 2. Comparison of segmentation techniques by measurements of density and volume of the tympanoperiotic complexes (TPC) in the adult male *Ziphius cavirostris*

	Technique	Density range (g/cc)	Density range width (g/cc)	Scan thickness (mm)	TOTAL TPC volume (cm^3)	LEFT TPC volume (cm^3)	RIGHT TPC volume (cm^3)
1	Threshold	1.50–2.87	1.37	1.5	97.91	47.32	50.50
2	Threshold	1.50–2.87	1.37	0.6	92.79	47.16	45.63
3	Threshold	1.69–2.98	1.29	0.6	79.04	38.31	40.73
4	Threshold	1.69–2.98	1.29	0.6	79.00	38.30	40.70
5	Threshold	2.16–2.98	0.82	0.6	50.70	25.90	24.80
6	Threshold	2.16–2.87	0.71	1.5	40.69	19.90	20.79
7	Computer + Human (TC) 7/30/05			1.5	83.91	42.78	41.13
8	Computer + Human (TC) 8/30/07			1.5	77.26	37.02	40.24
9	Computer + Human (TC) 1/18/06			0.6	68.52	33.60	34.92
10	Computer + Human (MM)			1.5	79.27	38.03	41.24

[a]Comparative segmentation measurements for the adult male *Ziphius* specimen as an indicator of error. The column labeled "Technique" indicates that we used two different methods to define tissue boundaries. The values in the Density Range column were translated from computed tomography (CT) numbers using the graph in Figure 1b. The Threshold technique was used to take the human out of the segmentation process, where the decisions about which volume elements (voxels) to include are based solely upon whether its density is within a pre-selected range. The table indicates the number of voxels or volume that is contained within the bony ear complexes (TPC) for various boundary definitions. The values obtained using only the threshold technique for different density ranges are shown in rows 1–6. Boundaries and the corresponding volumes defined by human observers using some computer-based image processing tools are shown in rows 7–9. Values in rows 7, 8, and 9 were calculated by the same person (T.C.) on different dates as indicated.

with the phonic lips. Immature animals also feature anatomic geometries that are allometrically distinct from adults, adding to the difficulty of making comparisons because of the differences in relative proportions.

Indications from years of experience dissecting specimens across a wide range of species, some with a large number of specimens, suggest that individual differences will not lead to significantly different interpretations or the general patterns described here. But in the final analysis, there will always be other possible interpretations based upon the small sample size and the fact that we included a neonate. Still, it seemed important to add, even incrementally, to the meager knowledge base on *Ziphius*, particularly in light of the fact that this species has stranded in higher numbers than any other species in incidents associated with exposure to high-intensity sound (Evans and England, 2001; MacLeod and D'Amico, 2005; Cox et al., 2006; Rommel et al., 2006).

Because structure and function are inextricably joined, it is reasonable to assume that the large, sexually dimorphic (structural) differences we see in the skulls, and probably the associated soft tissue nasal (sound transmission) anatomy of *Ziphius*, is evidence that we should see corresponding differences in acoustic function (Johnson et al., 2006). We might expect some sort of "acoustic signature" from the structural differences between conformations in the sound generation and propagation apparatus, that is, the large fat-filled basin in males but not in females. This brings to mind the notion of "acoustic sexual selection" (Cranford, 1999), which attempts to explain the function of the greatly hypertrophied spermaceti organ and the sexually dimorphic anatomy in the forehead of the sperm whale. Can we extrapolate this idea to include *Ziphius*? At this juncture, we suspect that the ASO in *Ziphius* may be functionally equivalent or "analogous" to the spermaceti organ in the sperm whale. In 2005, McKenna provided the first quantitative comparisons of the fat bodies in the foreheads of odontocetes (McKenna, 2005). These kinds of comparative studies should lead us to explanations of functional differences.

It is reasonable to assume that *Ziphius*, along with all other odontocetes produce their biosonar signals in the forehead using homologous structures, a concept known as the "unified hypothesis" (Cranford et al., 1996). Oddly enough, Zimmer and his colleagues (2005a) have recorded sonar signals from *Ziphius* that are unlike most delphinid signals in that they appear similar to a brief frequency upsweep often seen in FM bats. The mechanism for the production of these signals is currently unexplained, but it is likely that the apparatus used to generate them is consistent across the Odontoceti (Cranford et al., 1996; Johnson et al., 2006).

There are at least two "tests" of where sonar sounds are generated in *Ziphius*. Because we expect different sounds to emanate from different forehead configurations, then we may find detectable differences between high-fidelity acoustic recordings of adult males and females. Such recordings may already exist. Mark Johnson and his colleagues at Woods Hole Oceanographic Institution have collected a plethora of recordings from a variety of odontocetes, including ziphiids and sperm whales (Madsen et al., 2002a,b, 2004; Johnson and Tyack, 2003b; Johnson et al., 2004; Zimmer et al., 2005a,b; Johnson et al., 2006).

Another interesting "test" of acoustic function within the head of *Ziphius* could make use of finite element modeling (FEM) techniques (Krysl et al., 2007). For example, one intriguing question is: What is the function of an ASO that is encased in the high-density rostral bones? It would appear that this arrangement would

result in sounds being "trapped" inside the ASO or perhaps "guided" by the high-density bony boundaries. This may be similar to the function of the dense connective tissue case that bounds the spermaceti organ in sperm whales (Norris and Harvey, 1972; Cranford, 1999). Studies of several odontocete species have shown that the transmitted sonar beam emanates from the melon (Schevill and Watkins, 1966; Norris and Evans, 1967; Au, 1980, 1993; Au et al., 1986, 1988, 1995, 2006). By extension, it must be the same in *Ziphius*, but then how does sound get from the ASO to the melon? These questions, and many others, can be addressed using FEM techniques. These techniques can be used to simulate acoustic propagation pathways and, by inference, the site of sound generation in the head of *Ziphius*. They can also be used to investigate sound reception pathways and the potential effects of high-intensity sounds. These studies are already under way (Cranford et al., in press).

Even if we accept that the ASO in *Ziphius* may be functionally equivalent or "analogous" to the spermaceti organ in the sperm whale, it is difficult to make convincing argument that the two structures are homologous (Norris and Harvey, 1972), considering that these structures appear to be in different positions with respect to the main nasal passage. It would be useful to know what types of lipids are represented in the various fat bodies. Identifying the various lipid fractions will require sampling and chemical analysis as has been conducted on other odontocetes (Morris, 1973, 1975; Malins and Varanasi, 1975; Litchfield et al., 1976; Flewellen and Morris, 1978; Karol et al., 1978; Koopman et al., 2003, 2006; Koopman, 2007).

There are a few observations that support the conditional acceptance of Norris and Harvey's (1972) suggestion that *Ziphius* has a lipid organ (ASO) that is homologous to the spermaceti organ (SO) in sperm whales. For example, both lipid structures (ASO & SO) terminate at the phonic lips. The phonic lips probably represent the ancient external closure of the nasal openings that have invaginated over evolutionary time so that the phonic lips are now located just inside the external nasal closure, the blowhole (K.S. Norris, personal communication). The phonic lips are designated as the source of sonar signals in every odontocete that has been investigated (Cranford et al., 1996; Cranford, 1999; Cranford and Amundin, 2003).

The ASO and SO both have an average lower density and, in dissection, appear different in reflected light when compared with the melon or junk. Another common feature is that the SO and the ASO are horn-shaped (Zimmer et al., 2005c), broad posteriorly and narrowing or tapering anteriorly (Figs. 5a,b, 7b). Volumetrically, the ASO and the SO are second only to their associated skulls, making them prominent structurally, physiologically expensive, and most likely functionally significant (Cranford, 1999; Møhl et al., 2000; Møhl et al., 2003a and 2003b).

There are some significant differences between the ASO and the SO. Primary among them, the ASO is nestled in the skull and below the melon in *Ziphius*, but we see this arrangement upside down in *Physeter*, where the junk (homologue of the melon) sits upon the dorsal aspect of the bony rostrum and the SO is dorsal to the junk (Norris and Harvey, 1972; Cranford, 1999, 1992). It is also noteworthy that, even though the phonic lips are connected to the tapered ends of the lowest density fat body in both species, these locations are at opposite ends of the forehead (primarily because of the extreme torsion within *Physeter*; Klima, 1987; Cranford, 1992). The region of contact between the melon and the low density fat bodies (ASO & SO) along with the terminal phonic lips leads us to believe that the acoustic functions in the ASO & SO may be similar. The precise mechanism(s) of the functionality and the extent of potential functions have not been resolved. Still, our CT studies and dissections indicate that the ASO of the adult male *Ziphius* is not homologous to the SO of the sperm whale because of its relationship to prominent nearby landmarks such as the spiracular cavity.

One reason that it is difficult to distinguish these two components in the female is probably due to the lesser degree of tissue differentiation in neonates. The development of the odontocete melon is not likely to be complete in a neonate, because lipid moieties and concentrations tend to be quite different in adults (Koopman et al., 2003; Koopman, 2007). This makes it difficult to distinguish between components in the neonate by methods such as density differences or appearance in reflected light. Lesser tissue differentiation in the neonate may also account for the fact that we do not see evidence of the posterior (left–right) bifurcation of the melon, contrary to what we see in all other odontocete specimens we have examined. The *average* density for the entire ASO is 0.84 g/cc^3 and the mean density of the melon is 0.87 g/cc^3 for our adult male *Ziphius* (Table 1). The density difference between these largely lipid structures is small (0.02 g/cc^3). One explanation may be that these density values are averages across large volumes (more than 2 liters for each lipid structure) within the head. In addition, these organs are not purely lipids but also contain connective tissue components. The difference between these structures is easy to distinguish in the scans, so we can rest assured that the difference is real, but it is difficult to know what is at the root of the density difference. For example, is the density difference due to varying lipid moieties or concentrations as shown in previous studies (Litchfield et al., 1973, 1976, 1979; Morris, 1975; Flewellen and Morris, 1978)? The density difference might also be indicative of a greater number of connective tissue fibers in the melon as compared to the ASO, as it appears in dissection. Specifying the source of the density difference between the ASO and the melon in the adult male Ziphius will require further study. Nailing down the connective tissue structure and lipid analysis in the *Ziphius* forehead look to be the most expedient and promising way forward.

Let us briefly consider the development of the *prenarial basin*, the depression on the superior aspect of the skull just anterior to the superior bony nares in adult males. At this point, we are uncertain as to exactly how the prenarial basin is formed. Heyning (1989a, page 297) surmised that the prenarial basin in *Ziphius* is formed by the "reabsorption of the premaxillaries, maxillaries, and vomer {bones} in this region." Heyning's notion was based on observations of prepared skulls and his dissections. He did not have the benefit of the 3D views that CT scanning provides. We see no evidence to support his suggestion that bone absorption is the mechanism by which the pre-

narial basin is formed. To the contrary, our view of 3D bony morphology suggests that the bones have been rearranged to some degree and became thicker and denser than surrounding bones. We suggest that the deepening cavity may have been formed as the fat body intrudes into the region, "pushing aside" the various bony elements (Fig. 3). That the bones of the basin are extremely dense or pachyosteosclerotic is also counterintuitive to the notion of bone absorption. A definitive answer to the question of how the *Ziphius* prenarial basin is formed will await ontogenetic work, perhaps along the lines of Milan Klima (Klima, 1987, 1995, 1999).

Steep density gradients or abrupt density changes at tissue interfaces can be valuable as acoustic refractors and reflectors. Air spaces function as nearly perfect acoustic mirrors at a water or tissue interface. Air sacs, sinuses, and cavities are common features in the heads of the Delphinoidea (oceanic dolphins) and the Platanistoidea (river dolphins) (Lawrence and Schevill, 1956; Schenkkan, 1971, 1972, 1973; Mead, 1975). The members of these groups are not known for their deep-diving prowess; in fact, most inhabit relatively shallow water environments.

The platanistoids inhabit mostly riverine and a few near-shore marine environments. Very little is known about the diving habits and limits of the oceanic dolphins but most of them inhabit coastal waters or the continental shelf, although a few species are more widely distributed or cosmopolitan. In these relatively shallow water environments, using air boundaries as acoustic mirrors is a plausible strategy. But in deep-diving odontocetes, where the hydrostatic pressure can be orders of magnitude greater than it is at the surface, any air volume is severely reduced and this limits the depths to which air-based acoustic reflectors can be effective.

As a consequence, air spaces are drastically reduced in the nasal regions of ziphiids (and sperm whales), in contrast to all other odontocete families. In the locations where we find nasal air passages and diverticula in delphinoids, we instead find dense connective tissue or pachyosteosclerotic bone in ziphiids. This finding suggests that acoustic mirrors based on air spaces are either nonessential or cannot be functionally maintained at depth for sound generation and beam formation operations. It also suggests that steep density gradients or interfaces between tissue types can be effective substitutes. The density disparity between compact bone and lipid tissue is the maximum attainable difference between tissues. We suspect that the very abrupt change between the low-density ASO and the high-density bones that embrace it are functionally significant, an idea that can be tested with finite element modeling tools (Sun et al., 2002; Richmond et al., 2005; Ross, 2005; Krysl et al., 2006, 2007).

Basicranial Anatomy

The combined structure of the peripheral auditory apparatus can be seen (Figs. 13, 14) as a suite of structures that converge (bones and fat bodies) upon and surround (air sinuses) the tympanoperiotic complex. These views make a plausible case for the "internal acoustic pinnae" (Fig. 13) formed by one or more of the following components: the external fat bodies (not pictured) overlying the posterior pan bones of the mandibles and forming part of Norris' acoustic window (Norris, 1968); the thinned translucent external wall of the pan bones; the internal mandibular fat bodies that conduct acoustic signals to specific locations on the TPC; and especially the air-filled sinuses (pterygoid, peribullary, and tympanic) that likely exclude acoustic stimuli from extraneous pathways and may focus or amplify sounds at specific locations. The analogy with the pinnae of other mammals may be imperfect and it is not unique (Norris, 1968). But from a systemic point of view, various combinations of these components of the peripheral auditory system likely serve functions often associated with avian or mammalian pinnae. They likely provide sound gathering, amplification, interaural time delays, binaural acoustic isolation, and hydrostatic pressure compensation functions for the hearing apparatus. The potential additional demands upon these functions during deep diving in the aquatic environment will be discussed further in the next section.

The anatomy of the air spaces on the ventral aspect of the *Ziphius* skull tells a very different story from the forehead. The pterygoid sinuses are very large when compared with those of the riverine or oceanic dolphins. For example, our adult male Ziphius has a PCBL of 4.33 m and a total pterygoid sinus volume of almost 3 liters (2.99) (Table 1). By contrast, our records show that an adult female *Orcinus orca*, the largest oceanic delphinoid, has a PCBL of 5.71 m and a total pterygoid sinus volume of just over 1 liter (1.14). These comparisons show that the male *Ziphius* is only 75% the size of the killer whale but it has almost 3 times the volume within the pterygoid sinuses. At the same time, we should remember that these volumes were measured in dead animals and thus cannot be assumed to be maximum or minimum values. But these values do appear (during dissection) to represent reasonable approximations of relative pterygoid sinus volumes between these two specimens from different taxonomic families and perhaps hint at functional significance.

The pterygoid sinuses are also confluent with a complex of sheet-like and finger-like projections of air spaces (peribullary sinuses) in and around the TPCs, forming acoustics shields or reflective boundaries along the medial and posterodorsal aspects of the bony ear complexes. These structures can function as exquisite sound mirrors that provide acoustic isolation of the TPCs and protection from self-made sounds originating in the nasal complexes. A concise explanation of the multifunction role of air in the hearing apparatus of a dolphin, and by extension all odontocetes, can be found in Ridgway and Au (1999) and Norris (1968).

We concur with Fraser and Purves (1960) that the pterygoid sinuses provide a reservoir of air that can be directed posteriorly into the peribullary sinuses as the animal dives. They emphasized the maintenance of the tympanic cavity for the proper operation of the ossicular chain. The FVP provides a passive means for corralling the air into the peribullary sinuses around the TPCs. Fraser and Purves (1960) write, "The air sacs themselves are so extensive that their contraction would cause disruption of the adjacent musculature were it not for the intervention of some space-filling mechanism. It seems that the fibro-venous plexus which surrounds the sacs is ideally suited for this purpose, because there

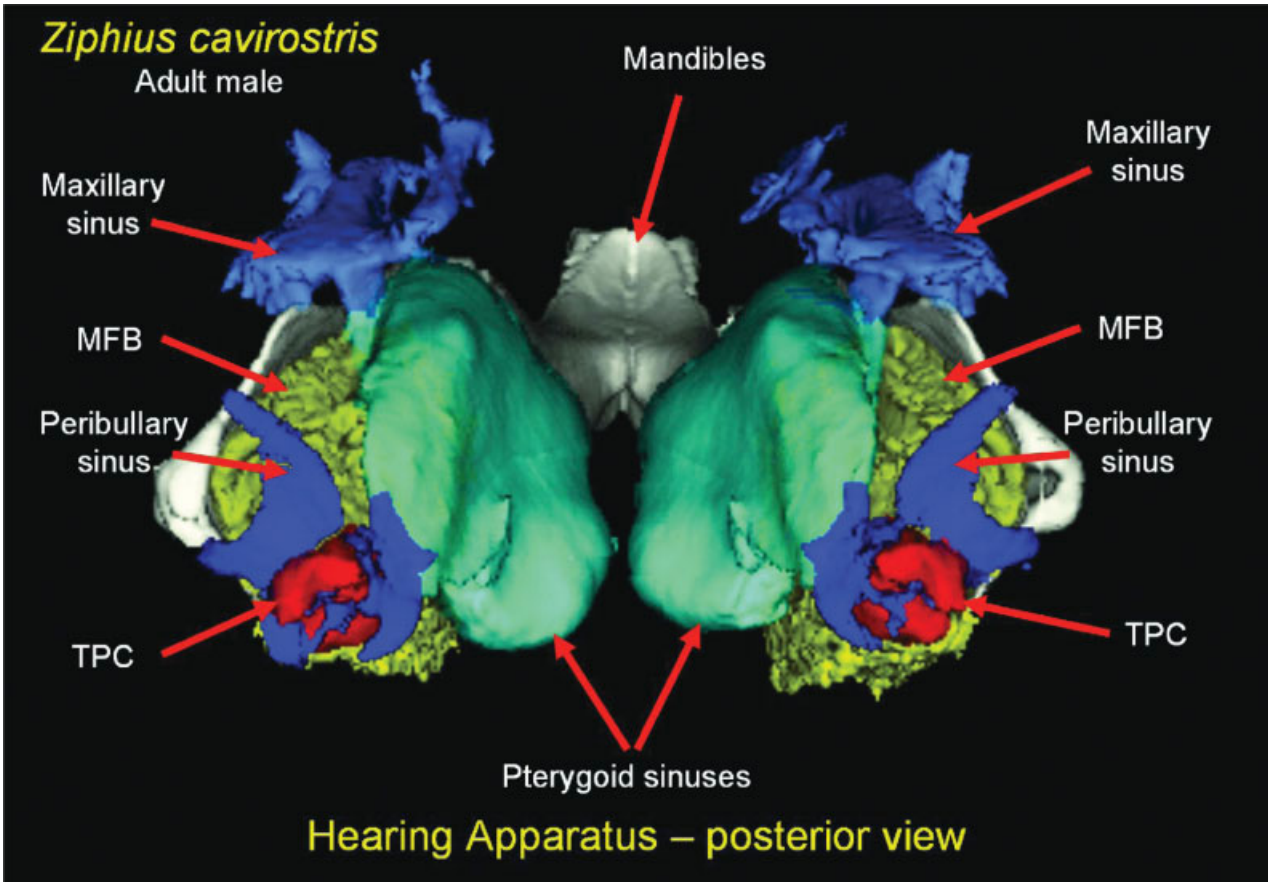

Fig. 13. Posterior view of the anatomic components of the "internal acoustic pinnae," part of the hearing apparatus in the adult male *Ziphius*. The posterior third ("pan bone") of the bony mandibles (white) are so thin that light and biosonar sounds can pass through them by an as yet undescribed mechanism (Norris, 1968). The internal mandibular fat bodies (MFB; yellow) fill the hollow region within the lower jaw and terminate on two lateral aspects of tympanoperiotic complexes (TPC; red). The air-filled pterygoid sinuses (cyan) are large and may serve as reservoirs to feed the maxillary sinuses (Dodger blue); the peribullary sinuses (blue), which form acoustic shields to isolate the TPCs from one another; as well as air for the tympanic cavity around the ossicles.

would be reciprocal filling of the plexus with reduction in the volume of the sinuses."

This is a passive mechanism, as the air volume in each pterygoid sinus is squeezed by the hydrostatic pressure, reducing its volume during diving, venous blood flows into the adjacent spaces of the FVP (Fig. 12), expanding its medial wall into the vacated sinus, and occluding or filling the space left by the collapsing air. The end result is that a small remaining volume of the air could be used to form the reflective acoustic mirror around each TPC to preserve binaural hearing or maintain an air-filled tympanic cavity, which allows efficient operation of the ossicular chain. This suggests that air is a precious commodity for deep-diving odontocetes and that there are probably mechanisms to make use of every bit.

We surmise that air sinuses in and around components of the hearing apparatus may be essential for it to function at peak performance but this does not necessarily mean that odontocete hearing would cease without some of them. In fact, one observation is pertinent to this topic. The character of the FVP changes from front to back. Anteriorly the structural elements of the FVP are thin, translucent, and gossamer-like (Fig. 12), so that most of the volume space could be filled with venous blood. Moving posteriorly, the character of the FVP changes gradually until most of the volume is composed of greatly thickened connective tissue walls, so that the blood containing spaces are reduced. One explanation for this dramatic change in the structure of the FVP is that when the hydrostatic pressure is great enough to compress the air of the neighboring peribullary sinus into a space too small to be functionally effective, there may still be enough reflectivity from the connective tissue layer of the FVP to serve the same functions at extreme depths. This finding may be one more example of how connective tissue can serve as a substitute for air spaces in deep-diving odontocetes.

Fraser and Purves (1960) maintain that a small bubble of air in the tympanic cavity is a prerequisite for hearing at depth. As a consequence, they proposed that the volume of the pterygoid sinuses might determine maximum dive depth. Fraser and Purves (1960, p.119) state, "It seems likely that the pterygoid air sinuses form a reservoir for this process of pressure regulation, and that the maximum depth to which the animal can dive is in relation to the ultimate compressibility of the air sacs and

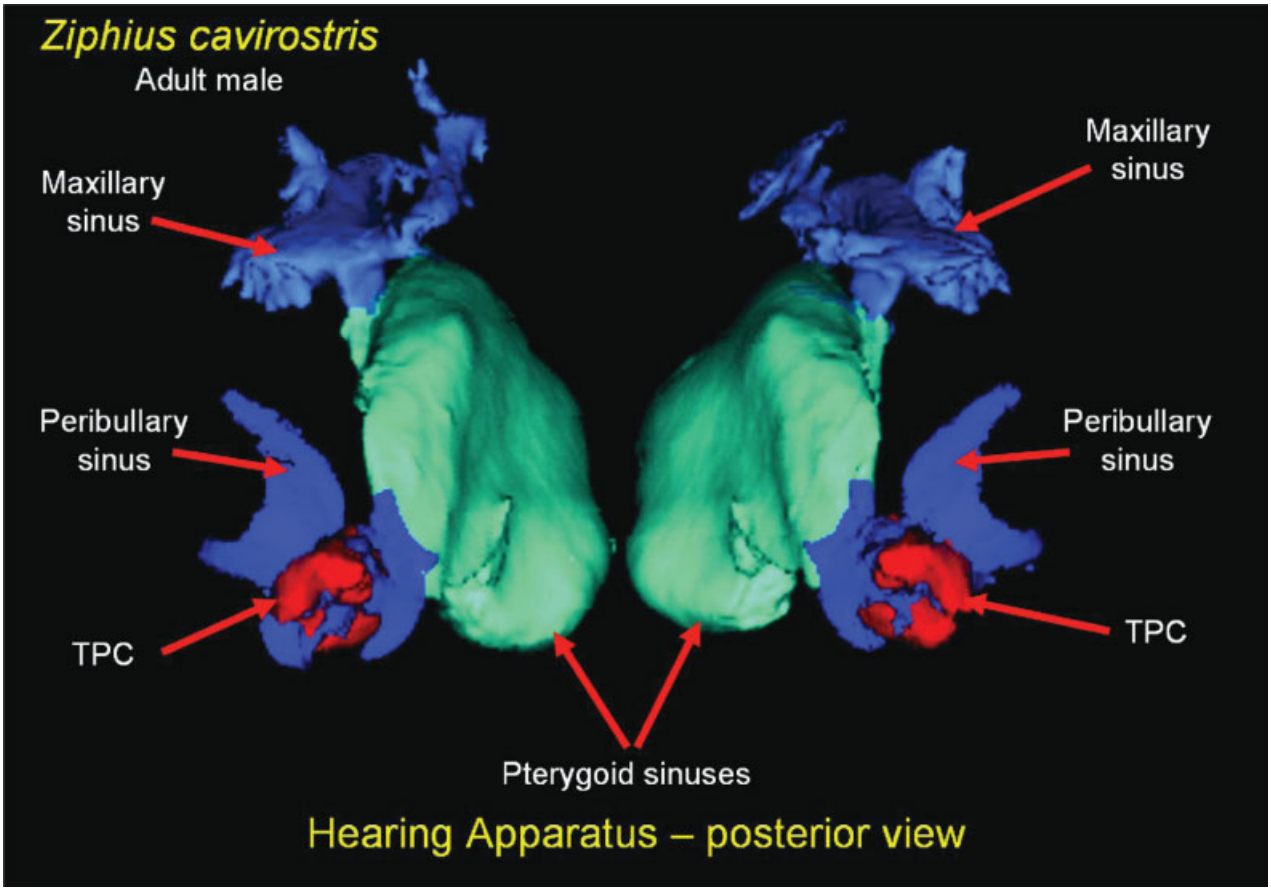

Fig. 14. The same posterior view as in Figure 13, except that the bony mandibles and mandibular fat bodies have been removed. What remains are the acoustically reflective air-filled sinuses, the large pterygoid sinuses (cyan), the maxillary sinuses (light blue), the peribullary and tympanic sinuses (blue), along with the bony tympanoperiotic complexes (TPC; red). These air spaces are essential functional components of the internal acoustic pinnae in deep-diving odontocetes.

the size of the tympanic cavity." Our volumetric results allow us to conduct a "thought experiment" on possible dive limits based upon the Fraser and Purves notion.

The volume of air in the right pterygoid sinus of our adult male is 1.5 liters, and the volume of the right peribullary sinus (including the tympanic cavity) is 35 ml. If we assume a constant (body) temperature, we can use Boyle's Law to calculate the amount of pressure required to compress 1,500 ml of air to 35 ml, a reduction factor of approximately 43. That value suggests, if the animal began with these spaces air-filled at the surface (1 ATM of ambient pressure), that it would take approximately 43 atmospheres of additional pressure to compress the entire volume of the pterygoid sinus into the volume of the peribullary sinus. If we use a conversion factor of approximately 10 m of depth equals 1 ATM of pressure increase; that translates to a depth of 430 m. As an estimate of the effect of diminishing air volume on the hearing apparatus, this should be considered a depth of minimum effect because the pressure relief surface of these air spaces need not be as thick as we find them in this postmortem specimen to function as a reflector. These animals clearly can dive much deeper, 1,888 m according to Tyack and his colleagues (2006).

Continuing this thought experiment, we measured the volume of the right tympanic cavity at almost 7 ml. Compressing the volume of the pterygoid sinus into the volume of the tympanic cavity requires approximately 214 atmospheres. This translates to a depth of approximately 2,140 m. In addition, we surmise that the volume of the tympanic cavity could be reduced by half and still contain an air bubble around the ossicular chain, although the mechanism for positioning the bubble is unclear. If the "essential" air volume is only 3 or 4 ml that corresponds to depths between 3,750 and 5,000 m, essentially no limit on dive depth. Again, it should be recognized that these numbers can only be viewed as a crude approximation gleaned from the anatomy of a postmortem specimen. At the same, our thought experiment seems to indicate that dive depth may be limited by the ratio of pterygoid sinus volume to tympanic cavity volume, as suggested by Fraser and Purves (1960).

The notion that maximum dive depth might be limited by pterygoid sinus volume is intriguing. But it does not preclude the caveat that hearing may well continue to function beyond the proposed limit, if in a diminished capacity. For example, the thickened interstitial connective tissue, as described for the posterior portion of the FVP, might function as a reflective boundary when the air volume at depth is too small to serve that function across the entire volume of the peribullary sinuses. The possible key role of the pterygoid sinuses is buttressed

by the fact that the deepest diving odontocetes (sperm whales and beaked whales) have the largest pterygoid sinuses, while shallow water species, like platanistoids, have reduced pterygoid sinuses. Unfortunately, the *maximum* volume of the pterygoid sinuses cannot be easily extracted from scans of dead specimens. The wall between the lateral pterygoid sinus and the adjoining FVP is membranous with considerable capacity for expansion. During the dissection, it appeared as if the pterygoid sinus was capable of expanding to at least twice the volume represented in the scans (perhaps as much as 6 liters total volume).

There is one curious result that deserves mention. The careful reader will note that the measured volume for the ears of the neonate is larger than that for the adult (Table 1). Accelerated development of the tympanoperiotic complexes in odontocetes has been reported previously (Yurick and Gaskin, 1987, 1988). Nevertheless, it seems rather odd that a neonate would have ears larger than an adult.

We were suspicious of this result so we collected segmentation information by three different methods for comparison. When we used a threshold-only method for segmenting the TPCs, we found that the ears of the adult are volumetrically slightly (23%) larger than that of the neonate. Inspection of the resulting segments revealed that this method did not capture the thinnest bony regions, of which there are many in odontocete TPCs. If these very thin bones are only a few pixels or less across, then the bones appear less dense because of scanner algorithms (Spoor et al., 1993). This finding means they will not be captured by a threshold-only process.

We also used the hands, eyes, and brains of two experienced operators combined with image processing techniques to segment the ears of the adult and neonate *Ziphius* specimens. These two independent, operator-determined volumes were similar and are those reported in Table 1. So, the question becomes, how do we interpret this odd result? There may be multiple contributing factors. The volume of the TPCs is small relative to the FOV, so any error will be magnified to some degree. In addition, the characteristics of bone in neonates and adults are normally very different, but perhaps less in this case considering the potential for accelerated development of the hearing apparatus. It has also been suggested that our curious result might be explained by the tendency for neonates to exhibit accelerated development of the brain and sensory systems resulting in enlarged features, perhaps for some sort of neurosensory "innate releasing mechanism" as espoused long ago by Konrad Lorenz (1935). This is perhaps not so preposterous in a deep-diving organism where most tissues are relatively transparent to their sonar sounds. An explanation of our conundrum remains equivocal and awaits future investigation.

Concluding Remarks

An important objective of this study was to demonstrate the value of quantitative image analysis. Digital images cry out for quantitative analysis but very often researchers do not take full advantage of this capacity. As we have shown, there are many advantages in using image analysis to understand functional morphology. For example, volume (a proxy for size), is an indicator of relative investment of resources, and perhaps functional importance. Digital images also allow us to define tissue boundaries quantitatively and, more importantly, provide morphology that is frozen in time so that comparisons can be made perennially with future specimens. Digital image analysis also provides a means for quantifying precision and/or error in our measurements. And finally, CT scans yield information that allows us to generate 3D density maps, which are important to understanding sound propagation.

Taken together, the biosonar anatomy in the head of *Ziphius* suggests one overriding theme that permeates most of the results reported here; acoustic reflectors are crucial. Air is a precious commodity in the life history of these prodigious diving mammals, but when air is unavailable a good substitute can be an interface of dense connective tissue or bone, particularly if it is an interface with acoustic fat.

A portion of this theme runs through the forehead where the dense connective tissue arch forms a waveguide or tunnel around the fatty melon, the anterior aperture of which is the only plausible pathway for sound emitted from the head (Figs. 2, 5–7). One critical role for air in the forehead is primarily in pressurizing and powering the sound generation process. Presumably, all odontocetes generate sonar signals in a similar manner using homologous structures, the "unified hypothesis" of Cranford et al. (1996). If we extrapolate the pattern seen in *Tursiops truncatus* (Cranford et al., 1997; Cranford, 2000; Cranford et al., In review) to all odontocetes, we find that only small bubbles of air are required to generate echolocation clicks. This must also be the case for the deep-diving Physeteroids, the sperm whales and beaked whales.

The other portions of the theme are prominent in association with the hearing apparatus on the underside of the head. Air plays a prominent role in maintaining the binaural properties of the hearing apparatus as previously discussed.

Because of its potential to be affected by exposure to high-intensity sound, the hearing apparatus is at the center of our interest here. It is possible that the cascade of events leading to stranding and death could begin with the tympanoperiotic complexes. At the same time, it is remarkable that we have a paucity of anatomic facts and incomplete understanding of the functional aspects of the hearing apparatus in odontocetes, some of the world's largest mammals. For example, there is a still debate about one of the most basic facets, whether the ossicular chain is a functional part of the conduction pathway (McCormick et al., 1970; Fleischer, 1980a; Ridgway et al., 2001).

In odontocetes, there are multiple acoustico-adaptations, including development of a novel acoustic pathway from the environment to the tympanoperiotic complex, thinned, translucent mandibles sandwiched between de novo fat bodies, enlarged pterygoid sinuses, increases in the density and stiffness of cochlear components, and an elongate basilar membrane, among others. Many of the bony elements have become almost porcelaneous and are often fused to one another. The connections between elements have been stiffened presumably to support high-frequency vibrations. All of these changes are used to receive, process, and analyze sound. Are there deleterious effects on these structural complexes by high-intensity sound?

Unfamiliarity is often an obstacle to gaining knowledge and understanding of a creature or system. Odontocetes spend the majority of their lives in an underwater world where light barely penetrates the surface layers and where vision, our most acute sense, is of limited value. The primary sensory modality in odontocetes is the hearing apparatus, but the wholesale evolutionary revamping of its architecture makes it as unfamiliar as the world in which these animals live. By definition, ziphiids are unfamiliar. The purpose of the work reported here is to pull back the veil of unfamiliarity for this little-known species and lay the groundwork for simulating and visualizing sound propagation pathways within the head. This investigative trajectory should bring us closer to understanding the biosonar apparatus and the effects of high-intensity sound on these animals.

ACKNOWLEDGMENTS

Several institutions, corporations, and their resident individuals played significant roles in advancing the completion of this work. We thank: Sal Juarez, Randy Huber, and Art McCarty at Hill AFB; Scott Ohlwiler and Trent Neel at ARACOR; Steve Shultz at Shultz Steel Inc.; Robert Gisiner at The Office of Naval Research; Frank Stone and Ernie Young at the Chief of Naval Operations (CNO 45); the Marine Mammal Commission; and Charley Potter, James Mead, and Dee Allen at the Smithsonian Institution, all provided critical help, support, and encouragement. We also thank several individuals for their efforts to move this project forward; Zoey Zahorodny, Caroline Harper, Kathy Langan-Cranford, Chris Garsha, and Allan Sauter for myriad and varied forms of support. In addition, we appreciate the excellent job by the professional photographers at the Smithsonian Institution (Chip Clark, Don Hurlbert, Ken Rahaim, and crew) for documenting the dissection of the adult male Ziphius. Susan Chivers at the National Marine Fisheries Service (SWFC) provided access to the neonate female specimen. We are immensely grateful to Debbie Duffield at Portland State University, she generously provided immediate, long-term, and repeated access to the adult male specimen. There is one more person we would like to recognize because his swift action and contribution were considerable enough to be invited as a coauthor. He graciously declined our invitation, indicating that his actions were merely in the line of duty. Those of us who struggle, often in vain, to obtain specimens in good condition of little-known species, will recognize the contribution. When the adult male specimen stranded, Ken Balcomb witnessed the event and recognized the potential value of this specimen. He sprang into action and obtained enough ice to cover the head until the salvage team could collect and process the specimen. His actions undoubtedly preserved the pristine condition of this specimen and provided a rare opportunity for study. We owe and acknowledge a debt of immense gratitude for his selfless acts from which we have greatly benefited. It should also be pointed out that because this specimen has been "perpetually preserved" by CT scanning, this specimen and Ken Balcomb's actions continue to contribute to our research efforts and will do so for years to come. At various stages during the development of this paper, colleagues accepted the Herculean task of reading and critiquing its contents. They greatly improved the final product, and we appreciate the efforts of Mats Amundin, Ann Pabst, and two anonymous reviewers. Still, any persistent errors or shortfalls remain the responsibility of the principal investigator.

LITERATURE CITED

Ackman RG, Eaton CA, Litchfield C. 1971. Composition of wax esters, triglycerides and diacyl glyceryl ethers in the jaw and blubber fats of the Amazon River dolphin (Inia geoffrensis). Lipids 6:69–77.

Ackman RG, Sipos JC, Eaton CA, Hilaman BL, Litchfield C. 1973. Molecular species of wax esters in jaw fat of Atlantic bottlenose dolphin, Tursiops truncatus. Lipids 8:661–667.

Amundin M. 1991. Helium effects on the click frequency spectrum of the harbor porpoise, *Phocoena phocoena*. J Acoust Soc Am 90:53–59.

Amundin M, Andersen SH. 1983. Bony nares air pressure and nasal plug muscle activity during click production in the harbour porpoise, *Phocoena phocoena*, and the bottlenosed dolphin, *Tursiops truncatus*. J Exp Biol 105:275–282.

Aroyan JL, Cranford TW, Kent J, Norris KS. 1992. Computer modeling of acoustic beam formation in *Delphinus delphis*. J Acoust Soc Am 92:2539–2545.

Au WWL. 1980. Echolocation signals of the Atlantic bottlenose dolphin (*Tursiops truncatus*) in open waters. In: Busnel RG, Fish JF, editors. Animal sonar systems. New York: Plenum Publishing Corporation. p 251–282.

Au WWL. 1993. The sonar of dolphins. New York: Springer-Verlag Inc.

Au WWL, Floyd RW, Haun JE. 1978. Propagation of Atlantic bottlenose dolphin echolocation signals. J Acoust Soc Am 64:411–422.

Au WWL, Moore PWB, Pawloski D. 1986. Echolocation transmitting beam of the Atlantic bottlenose dolphin. J Acoust Soc Am 80:688–691.

Au WWL, Penner RH, Turl CW. 1988. Propagation of beluga echolocation signals. In: Nachtigall PE, Moore PWB, editors. Animal sonar systems: processes and performance. New York: Plenum Publishing Corporation. p 47–51.

Au WWL, Pawloski JL, Nachtigall PE, Blonz M, Gisiner RC. 1995. Echolocation signals and transmission beam pattern of a false killer whale (*Pseudorca crassidens*). J Acoust Soc Am 98:51–59.

Au WWL, Kastelein RA, Benoit-Bird KJ, Cranford TW, McKenna MF. 2006. Acoustic radiation from the head of echolocating harbor porpoises (*Phocoena phocoena*). J Exp Biol 209:2726–2733.

Boisvert G. 2004. MRI properties of the head of a beaked whale. In: Oceanography. La Jolla: University of California, Department of Oceanography. p 79.

Bushberg JT, Seibert JA, Leidholdt EMJ, Boone JM. 2001. The essential physics of medical imaging. 2nd ed. Philadelphia: Lippincott Williams & Wilkins.

Cox TM, Ragen TJ, Read AJ, Vos E, Baird RW, Balcomb K, Barlow J, Caldwell J, Cranford T, Crum L, D'Amico A, D'Spain G, FernAndez A, Finneran J, Gentry R, Gerth W, Gulland F, Hildebrand J, Houser D, Hullar T, Jepson PD, Ketten D, MacLeod CD, Miller P, Moore S, Mountain DC, Palka D, Ponganis P, Rommel S, Rowles T, Taylor B, Tyack P, Wartzok D, Gisiner R, Mead J, Benner L. 2006. Understanding the impacts of anthropogenic sound on beaked whales. J Cetacean Res Manage 7:177–187.

Cranford TW. 1992. Functional morphology of the odontocete forehead: implications for sound generation. Santa Cruz: University of California, Department of Biology. p 276.

Cranford TW. 1999. The sperm whale's nose: sexual selection on a grand scale? Mar Mamm Sci 15:1134–1158.

Cranford TW. 2000. In search of impulse sound sources in odontocetes. In: Au WWL, Popper AN, Fay RR, editors. Hearing by whales and dolphins. New York: Springer-Verlag. p 109–156.

Cranford TW, Amundin ME. 2003. Biosonar pulse production in odontocetes: the state of our knowledge. In: Thomas JA, Moss CF, Vater M, editors. Echolocation in bats and dolphins. Chicago: The University of Chicago Press. p 27–35.

Cranford TW, Amundin M, Norris KS. 1996. Functional morphology and homology in the odontocete nasal complex: implications for sound generation. J Morphol 228:223–285.

Cranford TW, Van Bonn WG, Chaplin MS, Carr JA, Kamolnick TA, Carder DA, Ridgway SH. 1997. Visualizing dolphin sonar signal generation using high-speed video endoscopy. J Acoust Soc Am 102:3123.

Cranford TW, Elsberry WR, Bonn WGV, Carr JA, Chaplin MS, Blackwood DJ, Carder DA, Kamolnick T, Todd M, Ridgway SH. Observation and analysis of dolphin sonar signal generation. J Exp Biol (under review).

Cranford TW, Krysl P, Hildebrand J. Sound pathways revealed: simulated sound transmission and reception in Cuvier's beaked whale (*Ziphius cavirostris*). Bioinsp. Biomim (in press).

Evans DL, England GR. 2001. Joint interim report: Bahamas marine mammal stranding event of 15–16 March 2000. Washington, DC: US Department of Commerce & Secretary of the Navy. p 1–61.

Fleischer G. 1976. Hearing in extinct cetaceans as determined by cochlear structure. J Paleontol 50:133–152.

Fleischer G. 1980a. Low-frequency receiver of the middle ear in mysticetes and odontocetes. In: Busnel RG, Fish JF, editors. Animal sonar systems. New York: Plenum Publishing Corporation. p 891–893.

Fleischer G. 1980b. Morphological adaptations of the sound conducting apparatus in echolocating mammals. In: Busnel RG, Fish JF, editors. Animal sonar systems. New York: Plenum Publishing Corporation. p 895–898.

Flewellen CG, Morris RJ. 1978. Sound velocity measurements on samples from the spermaceti organ of the sperm whale (*Physeter catodon*). Deep Sea Res 25:269–277.

Fraser FC, Purves PE. 1960. Hearing in cetaceans: evolution of the accessory air sacs and the structure and function of the outer and middle ear in recent cetaceans. Br Mus (Nat Hist) Bull Zool 7:1–140.

Green RF, Ridgway SH, Evans WE. 1980. Functional and descriptive anatomy of the bottlenosed dolphin nasolaryngeal system with special reference to the musculature associated with sound production. In: Busnel RG, Fish JF, editors. Animal sonar systems. New York: Plenum Publishing Corporation. p 199–238.

Heyning JE. 1989a. Comparative facial anatomy of beaked whales (Ziphiidae) and a systematic revision among the families of extant Odontoceti. Contrib Sci Los Angeles County Mus 405:1–64.

Heyning JE. 1989b. Cuvier's beaked whale *Ziphius cavirostris* G. Cuvier, 1823. In: Ridgway SH, Harrison R, editors. Handbook of marine mammals. Vol. 4. River dolphins and the larger toothed whales. San Diego: Academic Press. p 289–308.

Hooker SK, Baird RW. 1999. Deep-diving behaviour of the northern bottlenose whale, Hyperoodon ampullatus (Cetacea: Ziphiidae). Proc R Soc Lond B 266:671–676.

Johnson M, Tyack P. 2003a. A digital acoustic recording tag for measuring the response of wild marine mammals to sound. J Ocean Eng 28:3–12.

Johnson MP, Tyack PL. 2003b. A digital acoustic recording tag for measuring the response of wild marine mammals to sound. IEEE J Ocean Eng 28:3–12.

Johnson M, Madsen PT, Zimmer WM, de Soto NA, Tyack PL. 2004. Beaked whales echolocate on prey. Proc Biol Sci 271(Suppl 6):S383–S386.

Johnson M, Madsen PT, Zimmer WM, de Soto NA, Tyack PL. 2006. Foraging Blainville's beaked whales (*Mesoplodon densirostris*) produce distinct click types matched to different phases of echolocation. J Exp Biol 209:5038–5050.

Karol C, Litchfield C, Caldwell DK, Caldwell MC. 1978. Compositional topography of melon and spermaceti organ lipids in the pygmy sperm whale (*Kogia breviceps*): Implications for echolocation. Mar Biol 47:115–123.

Kasuya T. 1973. Systematic consideration of recent toothed whales based on the morphology of the tympano-periotic bone. Sci Rep Whales Res Inst 25:1–103.

Ketten DR. 2000. Cetacean ears. In: Au WWL, Popper AN, Fay RR, editors. Hearing by whales and dolphins. New York: Springer-Verlag. p 43–108.

Klima M. 1987. Morphogenesis of the nasal structures of the skull in the toothed whales (Odontoceti). In: Kuhn HJ, Zeller U, editors. Morphogenesis of the mammalian skull. Hamburg: Verlag Paul Parey. p 105–122.

Klima M. 1995. Cetacean phylogeny and systematics based on the morphogenesis of the nasal skull. Aquat Mamm 21:79–89.

Klima M. 1999. Development of the cetacean nasal skull. Adv Anat Embryol Cell Biol 149:1–143.

Koopman HN. 2007. Phylogenetic, ecological, and ontogenetic factors influencing the biochemical structure of the blubber of odontocetes. Mar Biol 151:277–291.

Koopman HN, Iverson SJ, Read AJ. 2003. High concentrations of isovaleric acid in the fats of odontocetes: variation and patterns of accumulation in blubber vs. stability in the melon. J Comp Physiol B 173:247–261.

Koopman HN, Budge SM, Ketten DR, Iverson SJ. 2006. Topographical distribution of lipids inside the mandibular fat bodies of odontocetes: remarkable complexity and consistency. IEEE J Ocean Eng 31:95–106.

Krysl P, Cranford TW, Wiggins SM, Hildebrand JA. 2006. Simulating the effect of high-intensity sound on cetaceans: modeling approach and a case study for Cuvier's Beaked whale (*Ziphius cavirostris*). J Acoust Soc Am 120:2328–2339.

Krysl P, Cranford TW, Hildebrand JA. 2007. Lagrangian finite element treatment of transient vibration/acoustics of biosolids immersed in fluids. Int J Numerical Methods Eng DOI: 10.1002/nme.2192.

Lawrence B, Schevill WE. 1956. The functional anatomy of the delphinid nose. Bull Mus Comp Zool (Harvard) 114:103–151.

Litchfield C, Karol R, Greenberg AJ. 1973. Compositional topography of melon lipids in the Atlantic bottlenose dolphin (*Tursiops truncatus*): implications for echolocation. Mar Biol 23:165–169.

Litchfield C, Greenberg AJ, Caldwell DK, Caldwell MC, Sipos JC, Ackman RG. 1975. Comparative lipid patterns in acoustical and nonacoustical fatty tissues of dolphins, porpoises and toothed whales. Comp Biochem Physiol 50B:591–597.

Litchfield C, Greenberg AJ, Mead JG. 1976. The distinctive character of Ziphiidae head and blubber fats. Cetology 23:1–10.

Litchfield C, Karol R, Mullen ME, Dilger JP, Luthi B. 1979. Physical factors influencing refraction of the echolocative sound beam in delphinid cetaceans. Mar Biol 52:285–290.

Lorenz K. 1935. Der Kumpan in der Umwelt des Vogels. J Ornithol 83:137–215, 289–413.

MacLeod CD, D'Amico A. 2005. A review of knowledge about behaviour and ecology of beaked whales in relation to assessing and mitigating potential impacts from anthropogenic noise. J Cetacean Res Manage 7:211–221.

Madar SI. 1998. Structural adaptations of early archaeocete long bones. In: Thewissen J, editor. The emergence of whales. New York: Plenum Press. p 353–378.

Madsen PT, Payne R, Kristiansen NU, Wahlberg M, Kerr I, Møhl. B. 2002a. Sperm whale sound production studied with ultrasound-time-depth recording tags. J Exp Biol 213:1899–1906.

Madsen PT, Wahlberg M, Møhl B. 2002b. Male sperm whale (*Physeter macrocephalus*) acoustics in a high latitude habitat: implications for echolocation and communication. Behav Ecol Sociobiol 53:31–41.

Madsen PT, Kerr I, Payne R. 2004. Source parameter estimates of echolocation clicks from wild pygmy killer whales (*Feresa attenuata*) (L). J Acoust Soc Am 116:1909–1912.

Malins DC, Varanasi U. 1975. Cetacean biosonar: Part 2. The biochemistry of lipids in acoustic tissues. In: Malins DC, Sargent JR, editors. Biochemical and biophysical perspectives in marine biology. New York: Academic Press. p 237–287.

McCormick JG, Wever EG, Palin J, Ridgway SH. 1970. Sound conduction in the dolphin ear. J Acoust Soc Am 48:1418–1428.

McKenna MF. 2005. Comparative morphology of the odontocete melon: functional and evolutionary interpretations. San Diego: San Diego State University Biology Department. p 197.

McKenna MF, Goldbogen JA, St. Leger JA, Hildebrand JA, Cranford TW. 2007. Evaluation of postmortem changes in tissue structure in the bottlenose dolphin (*Tursiops truncatus*). Anat Rec 290:1023–1032.

Mead JG. 1975. Anatomy of the external nasal passages and facial complex in the Delphinidae (Mammalia: Cetacea). Smithson Contrib Zool 207:1–72.

Miller GS. 1923. The telescoping of the cetacean skull. Smithson Misc Coll 76:1–70.

Møhl B, Madsen PT, Wahlberg M, Au WWL, Nachtigall PE, Ridgway SH. 2003a. Sound transmission in the spermaceti complex of a recently expired sperm whale calf. J Acoust Soc Am Acoustics Research Letters Online 4:19–24.

Møhl B, Wahlberg M, Madsen PT, Heerfordt A, Lund A. 2003b. The monopulsed nature of sperm whale clicks. J Acoust Soc 114:1143–1154.

Møhl B, Wahlberg M, Madsen PT, Miller LA, Surlykke A. 2000. Sperm whale clicks: directionality and source level revisited. J Acoust Soc Am 107:638–648.

Morris RJ. 1973. The lipid structure of the spermaceti organ of the sperm whale (*Physeter catodon*). Deep Sea Res 20:911–916.

Morris RJ. 1975. Further studies into the lipid structure of the spermaceti organ of the sperm whale (*Physeter catodon*). Deep Sea Res 22:483–489.

Norris KS. 1964. Some problems of echolocation in cetaceans. In: Tavolga WN, editor. Marine bio-acoustics. New York: Pergamon Press. p 317–336.

Norris KS. 1968. The evolution of acoustic mechanisms in odontocete cetaceans. In: Drake ET, editor. Evolution and environment. New Haven: Yale University Press. p 297–324.

Norris KS. 1969. The echolocation of marine mammals. In: Andersen HT, editor. The biology of marine mammals. New York: Academic Press. p 391–423.

Norris KS. 1975. Cetacean biosonar: Part 1. Anatomical and behavioral studies. In: Malins DC, Sargent JR, editors. Biochemical and biophysical perspectives in marine biology. New York: Academic Press. p 215–234.

Norris KS. 1980. Peripheral sound processing in odontocetes. In: Busnel RG, Fish JF, editors. Animal sonar systems. New York: Plenum Publishing Corporation. p 495–509.

Norris KS, Evans WE. 1967. Directionality of echolocation clicks in the rough-tooth porpoise, *Steno bredanensis* (Lesson). In: Tavolga WN, editor. Marine bio-acoustics. New York: Pergamon Press. p 305–316.

Norris KS, Harvey GW. 1972. A theory for the function of the spermaceti organ of the sperm whale (*Physeter catodon* L.). In: Galler SR, Schmidt-Koenig K, Jacobs GJ, Belleville RE, editors. Animal orientation and navigation. Washington, DC: NASA Scientific and Technical Office. p 397–417.

Norris KS, Harvey GW. 1974. Sound transmission in the porpoise head. J Acoust Soc Am 56:659–664.

Omura H, Fujino K, Kimura S. 1955. Beaked whale *Berardius bairdi* of Japan, with notes on *Ziphius cavirostris*. Sci Rep Whales Res Inst 10:89–132.

Pouchet MG, Beauregard H. 1885. Sur "l'organe des spermaceti". Comptes Rendus de Socie'te' Biologique 11:343–344.

Richmond BG, Wright BW, Grosse I, Dechow PC, Ross CF, Spencer MA, Strait DS. 2005. Finite element analysis in functional morphology. Anat Rec 283A:259–274.

Ridgway SH. 1999. An illustration of Norris' acoustic window. Mar Mamm Sci 15:926–930.

Ridgway SH, Au WWL. 1999. Hearing and echolocation: dolphin. In: Adelman G, Smith B, editors. Encyclopedia of neuroscience. 2nd ed. Berlin: Springer-Verlag. p 858–862.

Ridgway SH, Carder DA, Green RF, Gaunt AS, Gaunt SLL, Evans WE. 1980. Electromyographic and pressure events in the nasolaryngeal system of dolphins during sound production. In: Busnel RG, Fish JF, editors. Animal sonar systems. New York: Plenum Publishing Corporation. p 239–250.

Ridgway SH, Carder DA, Kamolnick T, Smith RR, Schlundt CE, Elsberry WR. 2001. Hearing and whistling in the deep sea: depth influences whistle spectra but does not attenuate hearing by white whales (*Delphinapterus leucas*) (Odontoceti, Cetacea). J Exp Biol 204:3829–3841.

Robb RA. 1995. Three-dimensional biomedical imaging: principles and practice. New York: VCH Publishers, Inc.

Robb RA. 2000. Biomedical imaging, visualization, and analysis. New York: Wiley-Liss, Inc.

Rommel SA, Costidis AM, Fernandez A, Jepson PD, Pabst DA, McLellan WA, Houser DS, Cranford TW, van Helden AL, Allen DM, Barros NB. 2006. Elements of beaked whale anatomy and diving physiology, and some hypothetical causes of sonar-related stranding. J Cetacean Res Manage 7:189–209.

Ross CF. 2005. Finite element analysis in vertebrate biomechanics. Anat Rec 238A:253–258.

Schenkkan EJ. 1971. The occurrence and position of the "connecting sac" in the nasal tract complex of small odontocetes (Mammalia, Cetacea). Beaufortia 19:37–43.

Schenkkan EJ. 1972. On the nasal tract complex of *Pontoporia blainvillei* Gervais and d'Orbigny 1844 (Cetacea, Platanistidae). In: Pilleri G, editor. Investigations on Cetacea. p 83–90.

Schenkkan EJ. 1973. On the comparative anatomy and function of the nasal tract in odontocetes (Mammalia, Cetacea). Bijdr Dierk 43:127–159.

Schevill WE, Watkins WA. 1966. Sound structure and directionality in *Orcinus* (killer whale). Zoologica 51:71–76.

Silva M. 1998. Allometric scaling of body length: elastic or geometric similarity in mammalian design. J Mammal 79:20–32.

Soldevilla MS, McKenna MF, Wiggins SM, Shadwick RE, Cranford TW, Hildebrand JA. 2005. Cuvier's beaked whale (*Ziphius cavirostris*) head tissues: physical properties and CT imaging. J Exp Biol 208:2319–2332.

Spoor CF, Zonneveld FW, Macho GA. 1993. Linear measurements of cortical bone and dental enamel by computed tomography: applications and problems. Am J Phys Anthropol 91:469–484.

Sun Q, Gan RZ, Chang KH, Dormer KJ. 2002. Computer-integrated finite element modeling of human middle ear. Biomech Model Mechanobiol 1:109–122.

Tyack PL, Johnson M, Soto NA, Sturlese A, Madsen PT. 2006. Extreme diving of beaked whales. J Exp Biol 209:4238–4253.

Wever EG, McCormick JG, Palin J, Ridgway SH. 1971. The cochlea of the dolphin, *Tursiops truncatus*: hair cells and ganglion cells. Proc Natl Acad Sci U S A 68:2908–2912.

Yurick DB, Gaskin DE. 1987. Morphometric and meristic comparisons of skulls of harbour porpoise *Phocoena phocoena* (L.) from the north Atlantic and north Pacific. Ophelia 27:53–75.

Yurick DB, Gaskin DE. 1988. Asymmetry in the skull of the harbour porpoise *Phocoena phocoena* (L.) and its relationship to sound production and echolocation. Can J Zool 66:399–402.

Zahorodny ZP. 2007. Ontogeny and organization of acoustic lipids in jaw fats of the bottlenose dolphin (*Tursiops truncatus*). Wilmington, NC: University of North Carolina Department of Biology and Marine Biology. p 121.

Zimmer WM, Johnson MP, Madsen PT, Tyack PL. 2005a. Echolocation clicks of free-ranging Cuvier's beaked whales (*Ziphius cavirostris*). J Acoust Soc Am 117:3919–3927.

Zimmer WM, Madsen PT, Teloni V, Johnson MP, Tyack PL. 2005b. Off-axis effects on the multipulse structure of sperm whale usual clicks with implications for sound production. J Acoust Soc Am 118:3337–3345.

Zimmer WM, Tyack PL, Johnson MP, Madsen PT. 2005c. Three-dimensional beam pattern of regular sperm whale clicks confirms bent-horn hypothesis. J Acoust Soc Am 117:1473–1485.